RESEARCH ARTICLE

Conversion of Polyethylenes into Fungal Secondary Metabolites

Chris Rabot[a+], Yuhao Chen[b,c+], Swati Bijlani[a], Yi-Ming Chiang[a], C. Elizabeth Oakley[d], Berl R. Oakley[d], Travis J. Williams[b,c*], Clay C. C. Wang[a,b,c*]

[a] Department of Pharmacology & Pharmaceutical Sciences
University of Southern California
1985 Zonal Ave, Los Angeles, CA 90033
E-mail: clayw@usc.edu
[b] Donald P. and Katherine B. Loker Hydrocarbon Institute and Department of Chemistry
University of Southern California
837 Bloom Walk, Los Angeles, CA 90089
Email: travisw@usc.edu
[c] Wrigley Institute for Environmental Studies
University of Southern California
3454 Trousdale Parkway, Los Angeles, CA 90089
[d] Department of Molecular Biosciences
University of Kansas
1200 Sunnyside Avenue, Lawrence, KS 66045

[+] These authors contributed equally to this work.

Supporting information for this article is given via a link at the end of the document.

Abstract: Waste plastics represent major environmental and economic burdens due to their ubiquity, slow breakdown rates, and inadequacy of current recycling routes. Polyethylenes are particularly problematic, because they lack robust recycling approaches despite being the most abundant plastics in use today. We report a novel chemical and biological approach for the rapid conversion of polyethylenes into structurally complex and pharmacologically active compounds. We present conditions for aerobic, catalytic digestion of polyethylenes collected from post-consumer and oceanic waste streams, creating carboxylic diacids that can then be used as a carbon source by the fungus *Aspergillus nidulans*. As a proof of principle, we have engineered strains of *A. nidulans* to synthesize the fungal secondary metabolites asperbenzaldehyde, citreoviridin, and mutilin when grown on these digestion products. This hybrid approach considerably expands the catalog of products to which polyethylenes can be upcycled.

Introduction

Plastic production is currently accelerating at a rate faster than any other material on the planet,[1,2] and is estimated to reach a global production volume of 1.1 billion tons annually by 2040. Only 9% of plastics were recycled as of 2015.[3] Millions of tons of plastics, in the form of trillions of plastic particles,[4] leak from waste management systems into the environment, posing increasing threats to our food supply and ecosystems.[5] Generally, polyesters are frequently recycled (ca. 30% of polyethylene terephthalate (PET)), unlike polyolefins (ca. 6% of low-density polyethylene (LDPE)).[2,3] Due to their robust microstructures and excellent physicochemical properties, polyethylenes have been utilized to deliver countless improvements to quality of life and health. Polyethylenes are, thus, likely to remain ubiquitous in society. To minimize the environmental hazards they present, we must reclaim value embedded in these materials by developing viable upcycling approaches for them.

The same physicochemical properties that make polyethylenes useful also hinder their degradation and recycling. Further exacerbating this problem are additives that necessarily accompany any post-consumer waste stream, e.g. colorings and plasticizers. Unlike polyesters and nylons, the chemical methods known to recycle or remanufacture polyethylenes are limited. Some forcing methods (e.g. refluxing nitric acid, deep UV radiation) are known to cleave polyethylenes, the former to give carboxylic acids.[6-8] This type of strategy was exemplified in an oxidative process in which O_2 and nitric oxide (NO) were shown to cleave polyethylenes to carboxylic acids, nitrates, and other oxygenates at 170 °C and 40 atm with 65% total yield.[9]

Separately, oxidant-free, catalytic approaches are emerging for polyethylene upcycling, including alkane metathesis, hydrogenolysis, and related pathways to convert polyethylenes to light alkanes.[10,11] While these have modest yields and require energy-intensive conditions, they avoid the potential uncontrolled reactions that can result from heating organics with O_2. Still, oxidative conditions have the important advantage of tolerance to impurities associated with post-consumer polymer waste. These impurities, especially salts, are a particular concern in samples recovered from the oceans or recycling centers.

Chemical approaches to polyethylene degradation generate a diverse distribution of products because there are no functional handles in their pure hydrocarbon structures to direct a catalyst to where the polymer should be cleaved. We've shown, by contrast, that thermoset epoxies and fiber-reinforced polymers (FRPs) can be upcycled selectively, owing to the special chemistry of their linking nitrogen atoms.[12-14] In polyethylenes, the diversity of products arising from cleavage either limits the value of these products or creates a challenge of separating them. Thus, there is growing interest in employing biological systems to break down plastics.

Over the past two decades, several groups have made tremendous progress toward the biological upcycling of plastic degradation products. The discovery of enzymes capable of depolymerizing PET has inspired extensive interest in both PET degradation and upcycling.[15-18] Separately, whole-cell biocatalysts have also been employed to reclaim value embedded in PET. Several groups have demonstrated the microbe-facilitated generation of polyhydroxyalkanoates (PHAs) or related products from plastic-derived substrates.[19-21] Others have shown that PET-derived PHAs can be converted to both alkenoic acids and hydrocarbon fuels.[22] One group utilized *E. coli* to

convert PET-derived terephthalic acid into diverse aromatics, including gallic acid and catechol.[23] Others have engineered *E. coli* to upcycle terephthalic acid into vanillin.[24]

In contrast to PET, however, fewer biological upcycling approaches have been developed for polyolefins such as LDPE and HDPE. Recently, one group utilized *Pseudomonas putida* to biologically upcycle LDPE, in addition to other plastics, to PHAs and β-ketoadipate.[25] While several groups have investigated the chemical[26-28] and biological degradation of these polymers,[29-33] approaches to biologically valorize these polymers are limited.

We aimed to exploit fungi, which produce products worth billions of dollars each year[34] to biologically upcycle polyethylenes. Their biosynthetic products include medically valuable secondary metabolites (SMs) including antibiotics, the cholesterol-lowering statins, immunosuppressants, and antifungals.[35] Because they have been reported to use diacids as carbon sources,[36,37] we sought to generate structurally diverse and pharmacologically active SMs directly from polyethylene-derived substrates.

We show here that post-consumer polyethylenes can be rapidly degraded to generate substrates that are suitable for upgrading by fungal metabolism. As a proof of principle, we demonstrate that these plastic-derived substrates can be used to produce the diverse SMs asperbenzaldehyde, citreoviridin, and mutilin in useful yields (Scheme 1). We also demonstrate robust genetic engineering strategies that permit the expression of biosynthetic gene clusters (BGCs) from many different organisms. Thus, in principle, this method expands the catalog of products to which polyethylenes can be upcycled to thousands of SMs.

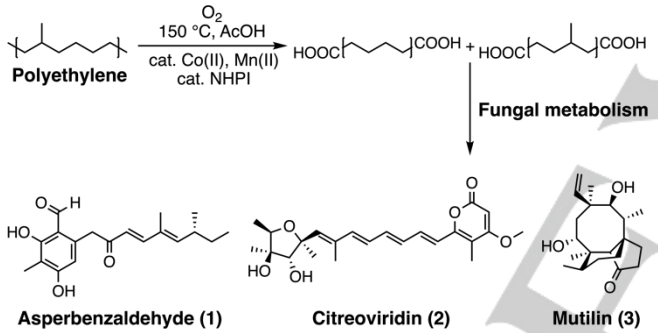

Scheme 1. The upcycling of polyethylenes to SMs. Polyethylenes are chemically degraded using metal catalysts and pressurized oxygen to generate a distribution of diacids, which are metabolized by fungi to rapidly produce structurally diverse SMs.

Results and Discussion

Optimization of Polyethylene Digestion

By adapting conditions for the conversion of cyclohexane to adipic acid,[38] we were able to optimize an initial system for polymer cleavage. Using O_2 consumption and ^{1}H NMR integration for indicative signals as our characterization handles (Fig. S1), we eventually found conditions based on cobalt and manganese salts and a phthalamide-based NO source[9] that give useful oxidative cleavage results (Table S1). The distribution of α,ω-diacid products that are produced by the oxidative chemistry was further be quantified by GCMS (see supplementary materials, Table S2 and Figs. S2-4).

We observed that re-charging our reactor with additional O_2 did not restart the polymer cleavage reaction and hypothesized that *N*-hydroxyphthalimide (NHPI) serves as a source of NO, which is vented from the reactor headspace upon O_2 recharge. We see rapid hydrolysis of NHPI to phthalic acid upon reaction initiation. We further observed that our metallic catalysts lost reactivity in the recharge process (Table S3, entries 4-6), and that a better result was obtained when metal salts were added portion-wise along with O_2 and NHPI at recharge (compare entries 6-7). Under conditions optimized for full polymer conversion to relatively small diacid products (Fig. S5), we observed 86 wt% mass recovery (entry 8) from a 5 g sample of clean polymer. Note that branched products were not tabulated in this yield, because they could not be unambiguously identified by identity to an authentic sample. Further, addition of oxygen to the polymer adds weight, so the molar yield of carbon atoms was 52% to the named products.

Its highly tolerant O_2-based conditions give this method the critical and distinguishing feature of tolerance of post-consumer wastes. We demonstrate that feature here with four examples (Fig. 1 & Table S4). Note that plasticizers and branched fragments from this LDPE film were omitted from the product accounting, although a large portion of these products are likely suitable for fungal digestion. A plastic grocery bag was homogenized into diacids of length C4-C12 with 34 wt% mass recovery, with an additional 2% of longer diacids (Table S4, entry 1). The balance of material comprises branched diacids derived from polymer branches, which are likely suitable for fungal metabolism. The bag must also contain colorings and plasticizers, which we account as non-products. A plastic milk jug and laboratory squeeze bottle (entries 2-3) were homogenized, respectively in 63 and 54 wt% mass recovery. These gave a distribution of products generally of higher mass than the grocery bag as shown in Figure 1B. The higher and lower recoveries are explained by the difference of HDPE versus LDPE: the HDPE milk jug does not have polymer branches that are omitted from the recovery calculation.

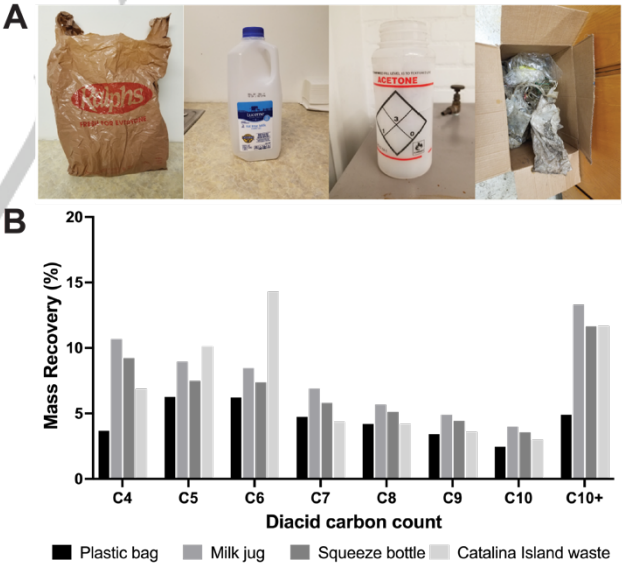

Figure 1. Post-consumer plastics degraded in this study. (A) From left to right: LDPE plastic grocery bag, HDPE milk jug, LDPE laboratory squeeze bottle, Pacific gyre waste collected from Santa Catalina Island, CA; (B) the distribution of diacid products after post-consumer polyethylene waste degradation using our optimized reaction.

Fungal Upgrading of Polyethylene Digestion Products

Fungi represent attractive candidates for diacid upgrading due to their robust growth capabilities, inexpensive cultivation requirements, engineerable metabolic pathways, and potential to synthesize metabolites with potent and diverse bioactivities. Short

chain diacids, however, have been reported to inhibit fungal growth.[39] We confirmed that C4-C8 (studied individually, Fig. S6)

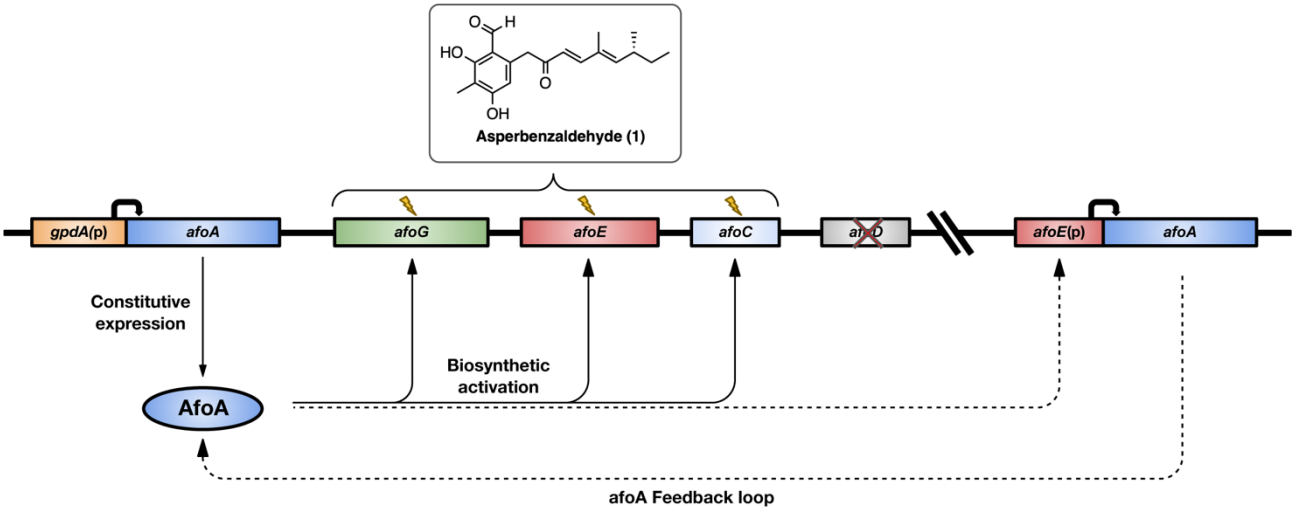

Figure 2. Overview of the novel promoter system driving production of asperbenzaldehyde in strain LO10050. The constitutive promoter *gpdA*(p) drives expression of *afoA*, encoding the AfoA transcription factor. AfoA binds to the promoter regions of genes *afoG*, *afoE*, and *afoC* within the asperbenzaldehyde BGC, leading to their expression and subsequent asperbenzaldehyde production. AfoA also binds to the *afoE* promoter (*afoE*(p)) controlling a second copy of *afoA* inserted elsewhere in the genome, driving additional AfoA production. This results in a positive feedback loop that generates high levels of both AfoA and asperbenzaldehyde. Note that *afoD* is deleted, halting conversion of asperbenzaldehyde to downstream metabolites. Other genes responsible for conversion of further downstream products to asperfuranone, the final product of the pathway, are not shown.

were toxic to the model filamentous fungus *A. nidulans* (strain FGSC A4) even when glucose was present as a carbon source. We found, however, that *A. nidulans* utilizes C10 and C12 diacids as sole carbon sources (Fig. S7) without signs of toxicity. We thus devised a system to separate polyethylene digestion products of ≥10 carbons from those <10 carbons. A series of pH-controlled liquid-liquid extractions permitted the rapid separation of C10+ diacids from light diacids and metal salts (Figs. S8-9).

In a representative example (vide supra), 27 wt% of ocean-sourced polyethylenes were converted to diacids that were discretely identifiable using authentic standards. It should be noted that light diacids are not waste products. They may be used in large-market applications such as in the synthesis of PBCx, a biodegradable plastic emerging in agricultural applications.[40] Our data also suggest that these light diacids possess antifungal properties (Fig. S6) that may be exploited.

For attempts to produce SMs from polyethylene-derived diacids, the heavy diacid extract was added to liquid minimal media at a concentration of 10 g L^{-1}. Liquid cultures were inoculated with fungal strains and incubated for several days (see ESI for a full extraction protocol, culture conditions, and media recipes). SMs were analyzed and quantified from culture extracts via HPLC-DAD and HPLC-DAD-MS.

Initial attempts to elicit SM production from various wild-type fungal strains resulted in only small amounts of SMs as detected via HPLC-DAD-MS. We consequently genetically engineered *A. nidulans* to overexpress SM biosynthetic genes or biosynthetic gene clusters (BGCs) and this proved effective, allowing robust and efficient SM production.

In order to determine the versatility of this system, we attempted to engineer fungal strains to produce various SMs using several BGC activation/expression approaches (Table S5). The SM used as a readout for the first of these systems was asperbenzaldehyde, a major polyketide intermediate in asperfuranone biosynthesis.[41] Asperbenzaldehyde and its derivatives disassemble tau filaments, inhibit lipoxygenases, and inhibit the interactions of the oncogenic RNA-binding proteins HuR and Musashi-1 with their target mRNAs.[42-44] We chose to target a biosynthetic intermediate because it can serve as a discovery platform that can easily be synthetically modified.

We developed three strains with different systems for driving asperbenzaldehyde production: LO2955, LO8355, and LO10050. All molecular genetic modifications were executed using previously described fusion PCR-based construct generation and transformation protocols.[45] In strain LO2955, the *afoD* gene was deleted, blocking asperfuranone biosynthesis such that asperbenzaldehyde, its biosynthetic precursor, accumulates. Further, the promoter of the *afoA* gene that encodes the transcription factor (AfoA) that drives expression of the asperfuranone BGC was replaced with the *alcA* promoter (*alcA*(p)), which is highly inducible with a variety of alcohols and ketones, including methyl ethyl ketone.[46] To increase expression of AfoA, we next replaced the promoter of the *alcR* gene with the strong, constitutive *gpdA* promoter[47] in LO2955, creating strain LO8355. The *alcR* sequence encodes a transcription factor that drives expression of *alcA*.[48]

In addition, we developed a new, strong constitutive promoter system that employs a positive feedback loop (Fig. 2) and incorporated it in strain LO10050. This system requires no induction and should drive strong expression on any carbon source, whereas the AlcA system is repressed by a number of sugars including glucose. The positive feedback system is designed to drive very high levels of transcription. In addition to the new promoter system and the deletion of *afoD*, LO10050 also carries deletions of the entire sterigmatocystin BGC (genes AN7804-AN7825) and the emericellamide BGC (genes AN2545-AN2549). Deletion of these highly expressed BGCs increases the pool of SM precursors, which are then free to feed into asperbenzaldehyde biosynthesis.

Yields of each strain grown in liquid lactose minimal media (LMM) were quantified via HPLC-DAD (Fig. S10). Each strain gave substantial yields but yields from LO10050 were the highest (4.3 g L^{-1} from 15 g L^{-1} lactose, or 29% mass conversion of lactose to asperbenzaldehyde). We therefore selected this strain to assay for asperbenzaldehyde production on polyethylene digest.

To determine the general utility of the system, we also attempted to express the diterpene antibiotic platform mutilin from the basidiomycete *Clitopilus passeckerianus* and the F1-ATPase β-subunit inhibitor citreoviridin from *A. terreus* var. *aureus*.[49] Mutilin is an intermediate in the biosynthetic pathway for pleuromutilin, which binds to the peptidyl transferase center of the

bacterial ribosome, thus halting protein synthesis.[50] Mutilin is therefore an attractive platform for medicinal discovery efforts toward overcoming bacterial antibiotic resistance. Further, basidiomycetes are phylogenetically distant from ascomycetes such as *A. nidulans* and the ability to produce mutilin would indicate that this system works for BGCs from very diverse fungi. Citreoviridin is a potent mycotoxin that uncompetitively and noncompetitively inhibits ATP hydrolysis and ATP synthesis, respectively, by binding to the β-subunit of F1-ATPase.[51] Compounds in this class of mycotoxins have been investigated for the treatment of cancer.[52] In total, four genes from *A. terreus* var. *aureus* and five genes from *C. passeckerianus* were transferred into an *A. nidulans* recipient strain and placed under control of *alcA*(p) to generate robust producers of citreoviridin and mutilin, respectively.

Engineered fungal strains were incubated in liquid minimal media supplemented with 10 g L^{-1} polyethylene digest extracts (PMM, polyethylene minimal media). Culture media and/or mycelia were extracted with appropriate organic solvents (see Materials and Methods), which were then analyzed via HPLC-DAD or HPLC-DAD-MS (Fig. 3). Standard curves were generated (Figs. S11-13) using purified standards to quantify SM yields in PMM relative to glucose minimal media (GMM) or minimal media controls. SMs were purified from polyethylene digest cultures and confirmed via ^{1}H NMR (Figs. S15-17) and tandem MS (Figs. S18-20).

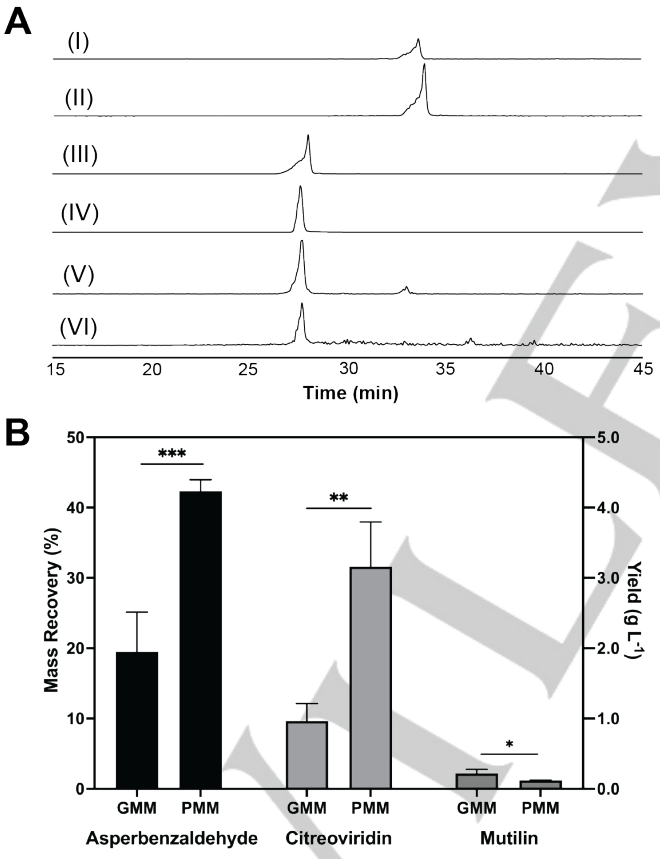

Figure 3. (A) Paired extracted ion chromatograms generated via HPLC-DAD-MS. Asperbenzaldehyde production in (I) GMM and (II) PMM; citreoviridin production in (III) GMM and (IV) PMM; mutilin production in (V) GMM and (VI) PMM. Intensities are normalized for metabolites in each condition (B) SM yields produced by engineered fungal strains when grown in PMM and GMM liquid media. Bars represent means ± SD (n = 3). *P ≤ 0.05; **P ≤ 0.01; ***P ≤ 0.005.

Our results indicate that engineered fungal strains can efficiently produce useful quantities of each target SM in under one week. Interestingly, microscopic examination of LO10050 when cultured in liquid PMM revealed initial stunted growth relative to GMM controls (Fig. S21). However, we observed ample hyphal growth after 48 hours and abundant asperbenzaldehyde crystals after 72 hours of incubation in PMM, which is consistent with our findings regarding asperbenzaldehyde titers.

These yields are in contrast to other metabolic engineering efforts; while high-yielding strains have been reported following extensive engineering,[53] ample SM production typically requires much larger quantities of carbon source(s) to achieve comparable yields.[54-56] It is also noteworthy that our yields were obtained from shake flasks with minimal optimization. Alteration of other culture parameters known to influence fermentation titers (e.g. culture length, media components, etc.) should permit significantly higher yields. Use of the strong constitutive promoter system may increase production of citreoviridin and mutilin and codon optimization may further increase mutilin production.

We further note that it was not necessary to employ metabolic engineering strategies to confer the ability to metabolize polymer-derived diacids to the fungi; rather, simple extraction protocols selectively isolated diacids suitable for fungal metabolism. Finally, it is quite likely that polyethylene degradation products can be used as a carbon source in the production of other SMs. The BGCs that we have expressed are from diverse fungi and the approaches we have developed should permit the expression of BGCs from many sources. The combination of the catalytic degradation of polyethylenes with genetic engineering of filamentous fungi represents a promising strategy to plastic upcycling.

Conclusion

We present a method to rapidly upcycle post-consumer polyethylenes into structurally diverse and medically useful SMs. We degrade these polyethylenes using oxidative catalysis to generate a distribution of diacids. These diacids are rapidly isolated and upgraded by engineered strains of *A. nidulans* to synthesize bioactive SMs. Taken together, this two-step process dramatically expands the catalog of products to which polyethylenes can be upcycled to thousands of SMs.

Acknowledgements

This study was funded by the National Science Foundation (CHE-1856395); the Department of Energy (Pacific Northwest National Laboratories subcontract); the University of Southern California (Dornsife College faculty working group, and Zumberge fund); the University of Southern California Wrigley Institute for Environmental Studies (Innovation award) and the University of Kansas Endowment (Irving S. Johnson Fund). This work was also supported by the Boy Scouts of America, Greater Los Angeles Area Council. We also thank LyondellBasell for providing model polyethylene pellets for initial polyethylene degradation and metabolism studies.

Keywords: catalysis • biosynthesis • polyethylenes • synthetic biology • upcycling

[1] U.S. Environmental Protection Agency (EPA), "Advancing Sustainable Materials Management: 2018 Fact Sheet", can be found under https://www.epa.gov/sites/default/files/2021-01/documents/2018_ff_fact_sheet_dec_2020_fnl_508.pdf, **2020**.
[2] D. E. MacArthur, *Science* **2017**, *358*, 843-843.
[3] R. Geyer, J. R. Jamback, K. L. Law, *Sci. Adv.* **2017**, *3*, e1700782.
[4] M. Eriksen, L. C. Lebreton, H. S. Carson, M. Thiel, C. J. Moore, J. C. Borerro, F. Galgani, P. G. Ryan, J. Reisser, *PloS One* **2014**, *9*, e111913.
[5] A. A. de Souze Machado, W. Kloas, C. Zarfl, S. Hempel, M. C. Rillig, *Glob. Change Biol.* **2018**, *24*, 1405-1416.
[6] L. R. Melby, *Macromolecules* **1978**, *11*, 50-56.

[7] A. Albertsson, S. Karlsson, *Polym. Degrad. Stab*. **1993**, *41*, 345-349.
[8] E. Backstrom, K. Odelius, M. Hakkarainen, *Ind. Eng. Chem. Res.* **2017**, *56*, 14814-14821.
[9] A. Pifer, A. Sen, *Angew. Chem. Int. Ed*. **1998**, *37*, 3306-3308.
[10] X. Jia, C. Qin, T. Friedberger, Z. Guan, Z. Huang, *Sci. Adv*. **2016**, *2*, e1501591.
[11] G. Celik, R. M. Kennedy, R. A. Hackler, M. Ferrandon, A. Tennakoon, S. Patnaik, A. M. LaPointe, S. C. Ammal, A. Heyden, F. A. Perras, M. Pruski, S. L. Scott, K. R. Poeppelmeier, A. D. Sadow, M. Deferro, *ACS Cent. Sci.* **2019**, *5*, 1795-1803.
[12] C. A. Navarro, Y. Ma, K. H. Michael, H. M. Breunig, S. R. Nutt, T. J. Williams, *Green Chem*. **2021**, *23*, 6356-6360.
[13] C. A. Navarro, E. A. Kedzie, Y. Ma, K. H. Michael, S. R. Nutt, T. J. Williams, *Top. Catal.* **2018**, *61*, 704–709.
[14] Y. Ma, C. A. Navarro, T. J. Williams, S. R. Nutt, S.R. *Polym. Degrad. Stab.* **2020**, *175*, 109-125.
[15] V. Tournier, C. M. Topham, A. Gilles, B. David, C. Folgoas, E. Moya-Leclair, E. Kamionka, M. L. Desrousseaux, H. Texier, S. Gavalda, M. Cot, E. Guémard, M. Dalibey, J. Nomme, G. Cioci, S. Barbe, M. Chateau, I. André, S. Duquesne, A. Marty, *Nature* **2020**, *580*, 216-219.
[16] B. C Knott, E. Erickson, M. D. Allen, J. E. Gado, R. Graham, F. L. Kearns, I. Pardo, E. Topuzlu, J. J. Anderson, H. P. Austin, G. Dominick, C. W. Johnson, N. A. Rorrer, C. J. Szostkiewicz, V. Copié, C. M. Payne, H. L. Woodcock, B. S. Donohoe, G. T. Beckham, J. E. McGeehan, *Proc. Nat. Acad. Sci.* **2020**, *117*, 25476-25485.
[17] R. Mueller, *Process Biochem.* **2006**, *41*, 2124-2128.
[18] R. Gao, H. Pan, L. Kai, K. Han, J. Lian, *World J. Microbiol. Biotechnol.* **2022**, *38*, 89.
[19] S. T. Kenny, J. N. Runic, W. Kaminsky, T. Wood, R. P. Babu, C. M. Keely, W. Blau, K. E. O'Connor, *Environ. Sci. Technol*. **2008**, *42*, 7696–7701.
[20] T. Tiso, T. Narancic, R. Wei, E. Pollet, N. Beagan, K. Schröder, A. Honak, M. Jiang, S. T. Kenny, N. Wierckx, R. Perrin, L. Avérous, W. Zimmermann, K. O'Connor, L. M. Blank, *Met. Eng.* **2021**, *66*, 167-178.
[21] D. Salvachúa, T. Rydzak, R. Auwae, A. De Capite, B. A. Black, J. T. Bouvier, N. S. Cleveland, J. R. Elmore, A. Furches, J. D. Huenemann, R. Katahira, W. E. Michener, D. J. Peterson, H. Rohrer, D. R. Vardon, G. T. Beckham, A. M. Guss, *Microb. Biotechnol.* **2020**, *13*, 290–298.
[22] J. G. Linger, D. R. Vardon, M. T. Guarnieri, E. M. Karp, G. B. Hunsinger, M. A. Franden, C. W. Johnson, G. Chupka, T. J. Strathmann, P. T. Pienkos, G. T. Beckham, *Proc. Nat. Acad. Sci.* **2014,** *111*, 12013–12018.
[23] H. T. Kim, J. K. Kim, H. G. Cha, M. J. Kang, H. S. Lee, T. U. Khang, E. J. Yun, D. H. Lee, B. K. Song, S. J. Park, J. C. Joo, K. H. Kim, *ACS Sus. Chem. Eng.* **2019**, *7*, 19396–19406.
[24] J. C. Sadler, S. Wallace, *Green Chem.* **2021**, 23, 4665-4672.
[25] K. P. Sullivan, A. Z. Werner, K. J. Ramirez, L. D. Ellis, J. R. Bussard, B. A. Black, D. G. Brandner, F. Bratti, B. L. Buss, X. Dong, S. J. Haugen, M. A. Ingraham, M. O. Konev, W. E. Michener, J. Miscall, I. Pardo, S. P. Woodworth, A. M. Guss, Y. Román-Leshkov, S. S. Stahl, G. T. Beckham, *Science* **2022**, *378*, 207-211.
[26] F. Zhang, M. Zeng, R. D. Yappert, J. Sun, Y. H. Lee, A. M. LaPointe, B. Peters, M. M. Abu-Omar, S. L. Scott, *Science* **2020**, *370*, 437–441.
[27] G. Celik, R. M. Kennedy, R. A. Hackler, M. Ferrandon, A. Tennakoon, S. Patnaik, A. M. LaPointe, S. C. Ammal, A. Heyden, F. A. Perras, M. Pruski, S. L. Scott, K. R. Poeppelmeier, A. D. Sadow, M. Delferro, *ACS Cent. Sci.* **2019**, *5*, 1795–1803.
[28] A. Tennakoon, X. Wu, A. L. Paterson, S. Patnaik, Y. Pei, A. M. LaPointe, S. C. Ammal, R. A. Hackler, A. Heyden, I. I. Slowing, G. W. Coates, M. Delferro, B. Peters, W. Huang, A. D. Sadow, F. A. Perras, *Nat. Catal.* **2020**, *3*, 893–901.
[29] C. F. Nnaji, E. C. Ogu, O. B. Akpor, *IOP Conf. Ser.: Mater. Sci. Eng.* **2021**, *1107*, 012135.
[30] S. D. Khandare, D. R. Chaudhary, B. Jha, *Biodegradation* **2021**, *32*, 127–143.
[31] M. S. Talkad, C. Chethan, S. Kavya, S. S. Qudsiya, S. Maria, A. Raj, A. Javed, *Int. J. Ethics Eng. Manag. Educ.* **2014**, *1*, 2348-4748.
[32] S. Awasthi, P. Srivastava, P. Singh, D. Tiwary, P. K. Mishra, *3 Biotech.* **2017**, *7*, 332.
[33] N. Ojha, N. Pradhan, S. Singh, A. Barla, A. Shrivastava, P. Khatua, V. Rai, S. Bose, *Sci. Rep.* **2017**, *7*, 39515.
[34] V. Meyer, M. R. Andersen, A. A. Brakhage, G. H. Braus, M. X. Caddick, T. C. Cairns, R. P. de Vries, T. Haarmann, K. Hansen, C. Hertz-Fowler, S. Krappmann, U. H. Mortensen, M. A. Peñalva, A. F. J. Ram, R. M. Head, *Fung. Biol. Biotech.* **2016**, *3*, 6.
[35] J. W. Bok, D. Hoffmeister, L. A. Maggio-Hall, R. Murillo, J. D. Glasner, N. P. Keller, *Chem. & Biol.* **2006**, *13*, 31–37.
[36] V. Côté, G. Kos, R. Mortazavi, P. A. Ariya, *Sci. Total Env.* **2008**, *390*, 530–537.
[37] D. Y. Kim, Y. H. Rhee, *Appl. Microbiol. Biotechnol*. **2003**, *61*, 300–308.
[38] Y. Ishii, K. Nakayama, M. Takeno, S. Sakaguchi, T. Iwahama, Y. Nishiyama, *J. Org. Chem*. **1995**, *60*, 3934-3935.
[39] H. Gershon, L. Shanks, *Can. J. Microbiol*. **1976**, *8*, 1198-1201.
[40] M. T. Zumsteinarno, A. Schintlmeister, T. F. Nelson, R. Baumgartner, D. Woebken, M. Wagner, H. P. Kohler, K. Mcneill, M. Sander, *Sci. Adv.* **2018**, *4*, eaas9024.
[41] Y. M. Chiang, E. Szewczyk, A. D. Davidson, N. Keller, B. R. Oakley, C. C. Wang, *J. Am. Chem. Soc.* **2009**, *131*, 2965–2970.
[42] S. R. Paranjape, Y. M. Chiang, J. F. Sanchez, R. Entwistle, C. C. C. Wang, B. R. Oakley, T. C. Gamblin, *Planta Med*. **2014**, *80*, 77–85.
[43] K. Kaur, X. Wu, J. K. Fields, D. K. Johnson, L. Lan, M. Pratt, A. D. Somoza, C. C. C. Wang, J. Karanicolas, B. R. Oakley, L. Xu, R. N. De Guzman, *PLoS One* **2017**, *12*, e0175471.
[44] L. Lan, J. Liu, M. Xing, A. R. Smith, J. Wang, X. Wu, C. Appelman, K. Li, A. Roy, R. Gowthaman, J. Karanicolas, A. D. Somoza, C. C. C. Wang, Y. Miao, R. De Guzman, B. R. Oakley, K. L. Neufeld, L. Xu, *Cancers* **2020**, *12*, 2221.
[45] E. Szewczyk, T. Nayak, C. E. Oakley, H. Edgerton, Y. Xiong, N. Taheri-Talesh, S. A. Osmani, B. R. Oakley, *Nat. Protoc.* **2006**, *1*, 3111–3120.
[46] E. H. Creaser, R. L. Porter, K. A. Britt, J. A. Pateman, C. H. Doy, *Biochem. J.* **1985**, *225*, 449-454.
[47] P. J. Punt, M. A. Dingemanse, B. J. Jacobs-Meijsing, P. H. Pouwels, C. A. van den Hondel, *Gene* **1988**, *69*, 49-57.
[48] B. Felenbok, D. Sequeval, M. Mathieu, S. Sibley, D. I. Gwynne, R. W. Davies, *Gene* **1988**, *73*, 385-396.
[49] Y. M. Chiang, T. S. Lin, S. L. Chang, G. Ahn, C. C. C. Wang, *ACS Synth. Biol*. **2021**, *10*, 173-182.
[50] S. M. Poulsen, M. Karlsson, L. B. Johansson, B. Vester, *Mol. Microbio.* **2001**, *41*, 1091–1099.
[51] E. M. Gause, M. A. Buck, M. G. Douglas, *J. Biol. Chem*. **1981**, *256*, 557–559.
[52] H. R. Park, I. J. Ryoo, S. J. Choo, J. H. Hwang, J. Y. Kim, M. R. Cha, K. Shin-Ya, I. D. Yoo, *Toxicology* **2007**, *229*, 253–261.
[53] J. Sun, H. S. Alper, *J. Ind. Microbiol. Biotechnol*. **2015**, *42*, 423–436.
[54] A. Li, N. Pfelzer, R. Zuijderwijk, P. J. Punt, *BMC Biotechnol.* **2012**, *12*, 57.
[55] A. Li, N. van Luijk, M. ter Beek, M. Caspers, P. Punt, M. van der Werf, *Fung. Gen. Biol.* **2011**, *48*, 6.
[56] S. Krull, A. Hevekerl, A. Kuenz, U. Prüße, *App. Microb. Biotech.* **2017**, 101, 4063-4072.

Entry for the Table of Contents

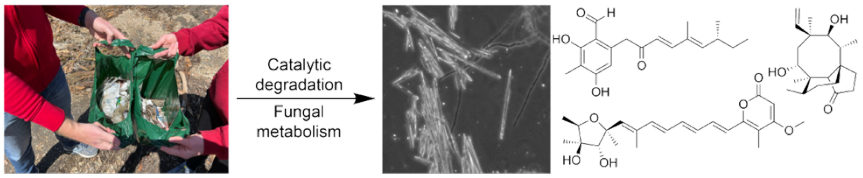

Mixed plastics were collected from Catalina Harbor on Catalina Island, CA. After sorting, polyethylenes were catalytically degraded into carboxylic diacids. These diacids are then upgraded by engineered strains of *Aspergillus nidulans* into structurally diverse secondary metabolites. Phase contrast micrographs show ample asperbenzaldehyde crystals in liquid culture medium containing polyethylene digest.

SUPPORTING INFORMATION

Table of Contents

Experimental Procedures

General methods

All commercially available chemicals were purchased from TCI America and used as received, except for cobalt nitrate and manganese nitrate, each obtained from Alfa Aesar. Acetic acid and hexanes were purchased from EMD Millipore. The NMR solvents chloroform-*d*, methanol-d_4, and acetone-d_6 were purchased from Cambridge Isotopes Laboratories. Solvents and metal salts were used as received.

Model low-density polyethylene was purchased from LyondellBasell (model LDPE, brand NA 270001) and used as received. The plastic grocery bag (LDPE), milk jug (HDPE) and acetone squeeze bottle (LDPE) were collected from the waste stream. The mixed plastic waste samples were collected from Catalina Harbor at Santa Catalina Island, CA. All the plastic waste samples were roughly washed and then shredded using a benchtop coffee grinder before use.

^{1}H NMR spectra were collected by Varian VNMRS 600 or 400MR spectrometers and processed via MestreLab Mnova. All the chemical shifts are shown by the units of ppm and referenced to the residual ^{1}H solvent peak; and line-listed according to (s) singlet, (d) double, (t) triplet, etc.

General procedure for catalyst screening

In a 300 mL Parr reactor, ground model LDPE powder (5 g) was mixed with NHPI (*N*-hydroxyphthalamide) and metal catalysts (0.5 g of each). Acetic acid (75 mL) was added to the mixture, and the Parr reactor was pressurized to 16 bars with oxygen and stirred at 150 °C. The reaction was manually terminated when no more oxygen consumption was observed as determined by change of reactor head pressure. Upon cooling to room temperature, the internal pressure of the reactor was released. The reactor was then recharged as described in the main text. At the conlucsion of conversion, volatiles including acetic acid were removed via distillation, and the reaction mixture was dissolved in 1 M NaOH solution (ca. 50 – 100 mL) and then filtered by vacuum filtration. The resulting translucent solution was acidified using concentrated HCl droplets to pH 1 and extracted with ethyl acetate (3 x 100 mL). The combined organic layers were dried over Na_2SO_4, and the solvent was removed by rotary evaporation to afford a yellowish, oily product mixture.

A known complication of our oxidative strategy is uncontrolled solvent oxidation:[1] this is a tradeoff between safety/scalability versus tolerance of impurities in the polymer waste stream. To scale these conditions, the process must operate at low enough O_2 pressure such that the vapor pressure of acetic acid is above its upper explosivity limit so that uncontrolled reactions cannot occur. Lowering O_2 pressure affords proportional reaction conversion (compare Table S3, entries 1-3), but not a decrease in reaction rate (entries 2-3). The system can be restarted by recharging the reactor with O_2 and catalysts (entry 4). These are consistent with a view that while [O_2] is not kinetically relevant, positive pressure is necessary to maintain catalyst life.

SUPPORTING INFORMATION

Safety notes: all pressurized reactions should be isolated behind appropriately rated blast shields and conducted at the minimal requisite scale. All reactions involving pressurized oxygen gas must have appropriately specified burst disks. All operations involving heating acetic acid should be conducted in a chemical fume hood. An analysis of upper and lower flammability limits should be conducted before heating any combination of oxygen gas and organic solvent. No scaling of such procedures should be attempted without consulting appropriate experts in safety engineering.

Analytical qualification and purification

In a representative analytical protocol, the obtained degradation product mixture was suspended in 100 mL methanol in a 250 mL round bottom flask, followed by adding a catalytic amount (ca. 20 uL) of concentrated H_2SO_4. A reflux condenser was placed on the flask and the mixture was stirred at 50 °C for 20 hours. Excess methanol was removed by distillation and the system was neutralized by adding $NaHCO_3$ powder until no gas evolution was seen. The residue was poured into diluted $NaHCO_3$ solution and extracted with ethyl acetate. The combined organic layers were dried over Na_2SO_4, and the solvent was removed under vacuum to afford a dark-yellow oil. The resulting mixture was dissolved in chloroform for mass-selective gas chromatography analysis (GC-MS, Agilent HP 6890 GC network with an Agilent 5973 mass selective detector).

The calibration curve (R^2 > 0.990 and standard error < 0.05) of each methanol-esterified product was generated by the corresponding standard dimethyl ester (C5 to C10 and C12; synthesized from the corresponding diacids, respectively) at different concentrations (500, 833, 1000, 1250 and 1428 ppm, respectively; *also see supplementary text section below*).

General procedure for condition optimization

To a 300 mL Parr reactor was added ground model LDPE powder (5 g), NHPI (0.5 g), cobalt nitrate (0.1 – 0.5 g), manganese nitrate (0.1 – 0.5 g) and acetic acid (75 mL). The reactor was pressurized with O_2 (2 - 18 bars, *see safety notes above*) and stirred at 150 °C. Once the pressure gauge reached zero bars, the reactor was removed from the heat and cooled to room temperature (50 – 60 min). The cooled reactor was then re-charged with O_2 and placed back to the heat to continue the reaction. After various cycles (see supporting tables), the reactor was cooled to room temperature and the remaining oxygen was released to the air once no further oxygen consumption was observed. The reactor was then opened, recharged with catalysts, sealed, pressurized back with O_2 and heated at 150 °C again to restart the reaction. After the reaction was completed, the resulting crude mixture was treated by the same work-up procedure as the initial studies to obtain a yellow-tinted, oily product mixture.

Digest purification/analyticals

Following ethyl acetate extraction, polyethylene digest was dried under vacuum, resuspended in 100 mL deionized H_2O, and pH-adjusted to 13.0 using 5.5 M KOH to maximize solubility. The solution was pH-adjusted to 8.0 using concentrated HCl (ca. 37% aq) and extracted with hexanes (3 x 1000 mL, technical grade), then further acidified to 1.0 and again extracted with hexanes (3 x 1000 mL). The combined hexane fractions were dried under vacuum and the obtained products were used to generate liquid media for fungal cultures.

Media recipes

All recipes are based on that of minimal medium (MM): 12.0 g L^{-1} $NaNO_3$, 3.04 g L^{-1} KH_2PO_4, 1.04 g L^{-1} KCl, 1.04 g L^{-1} $MgSO_4 \cdot 7H_2O$, and 1 mL L^{-1} Hutner's trace element solution.[2] MM is supplemented with 10 g L^{-1} d-glucose, lactose monohydrate, or polyethylene digest extract to create glucose minimal media (GMM), lactose minimal media (LMM), or polyethylene minimal media (PMM), respectively. Media was supplemented with riboflavin (2.5 mg L^{-1}), pyridoxine (0.5 mg L^{-1}), uracil (1.0 g L^{-1}), and/or uridine (10 mM) when necessary. For solid cultures, agar was added at a concentration of 1.5% w/v. For comparative metabolic experiments using liquid cultures, all media was pH-adjusted to 8.0 using 5.5 M KOH.

Diacid toxicity assay (GMM + diacids)

To determine the extent of toxicity of diacids of various chain lengths, 5.0 x 10^5 spores were inoculated into 24-well plates containing 2 mL of GMM plus 10.0, 1.0, and 0.1 g L^{-1} of diacid standards of length C4, 5, 6, 7, 8, 9, 10, and 12. Phthalic acid and NHPI were also included in the analysis. Diacids standards and catalysts were initially dissolved in 60 µL (3% v/v) DMSO. GMM, GMM + 3% v/v DMSO, MM, and MM + 3% v/v DMSO were used as controls. 24-well plates were incubated for seven days at 37 °C (Fig. S6).

Diacid uptake assay (MM + diacids)

To determine if *A. nidulans* can utilize diacids of various lengths as sole carbon sources, 1.0 x 10^6 spores were inoculated into 12-well plates containing 10 mL MM plus 10 g L^{-1} of diacid standards of length C4, 5, 6, 7, 8, 9, 10, and 12. Diacids standards were

initially dissolved in 300 µL (3% v/v) DMSO. GMM, GMM + 3% v/v DMSO, MM, and MM + 3% v/v DMSO were used as controls. 12-well plates were incubated for seven days at 37°C (Fig. S7).

Culture conditions

Spores (ca. 1.0 x 10^7) of each strain were inoculated into 25 mL Erlenmeyer flasks containing 10 mL of media. Cultures were incubated at 37°C with shaking at 180 rpm. In the case of YM192 and YM283, 50 mM methyl ethyl ketone (MEK) was added 42 hours after inoculation for *alcA*(p) induction. YM192 and YM283 were then incubated for an additional 72 hours. LO10050, which does not require induction, was incubated for a total of 144 hours. For comparative metabolomics experiment to determine relative production of asperbenzaldehyde, citreoviridin, and mutilin in PMM vs. GMM, all strains were cultured in triplicate.

Comparative metabolomics of asperbenzaldehyde-producing strains

Spores (ca. 3.0 x 10^7) of strains LO2955, LO8355, and LO10050 were inoculated in triplicate into 125 mL Erlenmeyer flasks containing 30 mL of GMM. Cultures were incubated at 37 °C for 144 hours with shaking at 180 rpm. For strains LO2955 and 8355, 50 mM methyl ethyl ketone (MEK) was added 42 hours after inoculation for *alcA*(p) induction.

Secondary metabolite analysis

For LO2955/LO8355/LO10050, 10 mL of methanol was added to culture flasks, which were then sonicated for one hour. Culture media with methanol was filtered and dried (TurboVap LV). Dried extracts were resuspended in 25 mL ddH_2O, which was extracted three times with 25 mL ethyl acetate. The organic phase was then dried, resuspended in 10 mL methanol, and diluted 1:99 in methanol. For YM192 and YM283, mycelia were filtered from the culture medium. The media was then extracted three times with 25 mL of dichloromethane (for YM192) or ethyl acetate (for YM283). Extracts were dried and resuspended in 10 mL methanol. Extracts from YM192 were diluted 1:9 in methanol. Extracts from YM283 were analyzed without further dilution.

Extracts of LO2955/LO8355/LO10050 and YM192 (10 µL each) were analyzed via HPLC-DAD (Agilent 1200 Series). Analysis was performed with an RP-18 column (Kinetex® 5 µm EVO C_{18} 100 Å LC Column, 150 x 4.6 mm) at a flow rate of 1.0 mL min^{-1} with detection using a DAD detector. The solvents for both asperbenzaldehyde and citreoviridin analysis were 100% AcN (solvent B) in 5% AcN−H_2O (solvent A), both with 0.05% TFA. For asperbenzaldehyde, the solvent gradient used was: 0 to 60% solvent B from 0 to 12 min, 60 to 100% solvent B from 12 to 15 min, 100% solvent B from 15 to 20 min, 100 to 0% solvent B from 20 to 21 min, and reequilibration with 0% solvent B from 21 to 26 min. For citreoviridin, the solvent gradient used was: 0 to 100% solvent B from 0 to 17 min, 100% solvent B from 17 to 22 min, 100 to 0% solvent B from 22 to 23 min, and reequilibration with 0% solvent B from 23 to 28 min.

As mutilin is not UV-active, 10 µL of YM283 culture extracts were analyzed via HPLC-DAD-MS. Spectra were acquired with a ThermoFinnigan LCQ Advantage ion trap mass spectrometer equipped with a reverse phase C_{18} column (Alltech Prevail C_{18}; particle size, 3 µm; column, 2.1 x 100 mm) with a flow rate of 125 µL min^{-1}. The solvents used were 95% AcN-H_2O (solvent B) in 5% AcN-H_2O (solvent A) plus 0.05% formic acid. The solvent gradient used was: 0% solvent B from 0 to 5 min, 0 to 100% solvent B from 5 to 35 min, 100% solvent B from 35 to 40 min, 100 to 0% solvent B from 40 to 45 min, and reequilibration with 0% solvent B from 45 to 50 min. MS conditions were as follows: 5.0 kV capillary voltage, sheath gas flow rate of 60 arbitrary units (AUs), auxiliary gas flow rate of 10 AUs, and ion transfer capillary temperature at 350 °C.

Standard curve generation

Purified standards of SMs were analyzed via HPLC-DAD (for asperbenzaldehyde and citreoviridin) or HPLC-DAD-MS (for mutilin). Each SM was injected at concentrations of 1.0, 0.3, 0.1, 0.03, and 0.01 g L^{-1} to generate standard curves (Figs. S11-13). Concentrations were plotted against AUCs for each metabolite. For mutilin, the measured AUC corresponded to a positive-mode extracted ion chromatogram (EIC) at m/z = 303, corresponding to the $[M+H-H_2O]^+$ ion. Microsoft Excel was used to generate standard curves, R^2 values, and regression formulae.

Compound purification

For asperbenzaldehyde purification, ethyl acetate extracts from LO10050 grown in 30 mL PMM were purified via HPLC-DAD equipped with a reverse phase C_{18} column (Luna C_{18}(2); 100 Å; 250 x 10 mm). The solvents used were 100% ddH_2O (solvent A) and 100% AcN (solvent B), both containing 0.05% trifluoroacetic acid with a flow rate of 4 mL min^{-1}. The solvent gradient was: 30% to 100% solvent B from 0 to 25 minutes, 100% solvent B from 25 to 30 minutes, 100% to 30% solvent B from 30 to 31 minutes, and reequilibration at 30% solvent B from 31 to 36 minutes. 13.3 mg of asperbenzaldehyde was isolated.

For citreoviridin purification, YM192 was cultured in 30 mL PMM. Extracts were purified via normal-phase preparative thin layer chromatography (Merck) using 3:1 ethyl acetate:hexanes as a mobile phase to yield 8.6 mg of citreoviridin.

For mutilin purification, YM283 was cultured in 200 mL PMM. Culture medium was extracted (vide supra), and extracts were purified via normal-phase preparative thin layer chromatography using 3:7 ethyl acetate:hexanes as a mobile phase to yield 7.1 mg of mutilin.

Results and Discussion

Product quantification

We thought it necessary accurately to quantify the distribution of α,ω-diacid products that are produced by the aerobic digest chemistry. We addressed this analytical problem by converting mixed diacid products resulting from aerobic polymer digestion to esters by acidic methanolysis to enable GC-MS analysis (Fig. S2). Products identified for linear diacids are readily assigned by mass and confirmed by identity to standard diester samples of the C5 (glutaric), 6 (adipic), 7, 8, 9, 10 and 12 diacids. Further, integration response factors can be calibrated for these seven known compounds, and uncertainties can be measured for each. Observing that these response factors are a linear function of carbon count with high co-variance (Pearson's $R^2 > 0.99$), we can predict with quantifiable certainty those response factors (eg. C11) for which we have no authentic sample (see Fig S3-4 & Table S2). Response factors for the inaccessible diesters are each within 2% standard error. Integration data from ^{1}H NMR, particularly for dimethyl phthalate, dimethyl succinate, and methylene groups adjacent to product esters groups enabled us to corroborate our GC assignments within the confidence of the NMR integration (d1 > 5 T1). This analysis neglects branched products resulting from pieces of LDPE that themselves contain branches.

Purification of C10+ diacids

Based on the observation that fungi utilize C10+ diacids as sole carbon sources, we chose to go forward with the less reactive oxidative system (Table S1, entry 6). In order to favor the generation of heavy diacids, we reduced the initial oxygen loading to 4 bars without any further recharging. In this case, 1.8 g of the initial 5.0 g model LDPE reacted after three hours. Following workup and pH-controlled liquid-liquid extraction, roughly 150-180 mg of heavy diacids were collected (confirmed by HPLC-DAD-MS, Figs. S8-9). Replacing model LDPE with oceanic waste resulted in the recovery of 200-220 mg of heavy diacids post-extraction. This extraction permitted the rapid and facile separation of C10+ diacids from diacids known to be toxic to the fungus. We observed that, following a final hexanes extraction of aqueous medium at pH 1, insoluble material that represented the majority of the ca. 1.8 g reacted starting material was also able to be utilized by fungi as carbon sources. We nevertheless chose to utilize the hexanes extracts for metabolomics experiments due to their absence of diacids C9 and below.

Figures

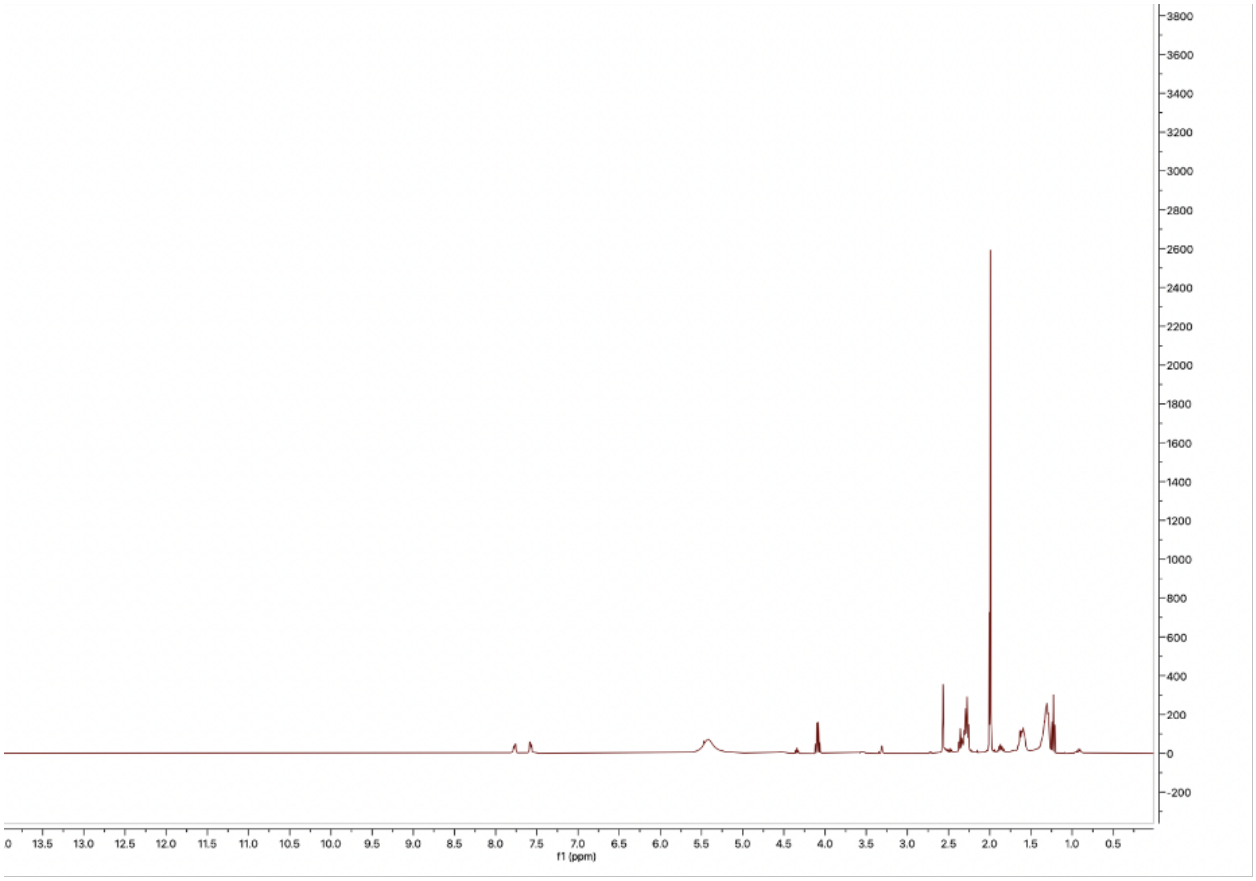

Figure S1. ^{1}H NMR showing evidence of symmetrical dicarboxylic acids. Dicarboxylic acids were dissolved in methanol-d_4.

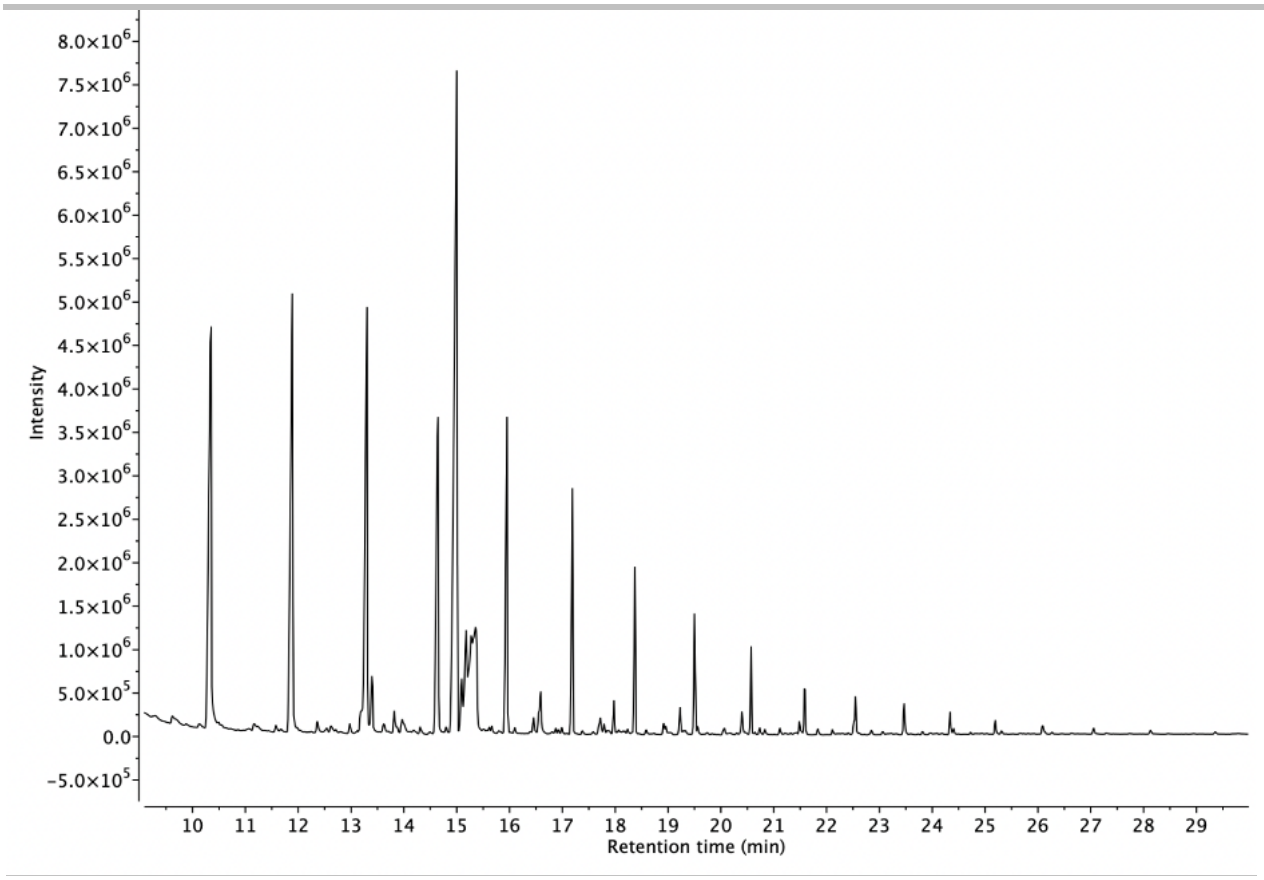

Figure S2. GC-MS spectrum showing methanol-esterified products of aerobic digestion (in chloroform). The tallest peak represents dimethyl phthalate.

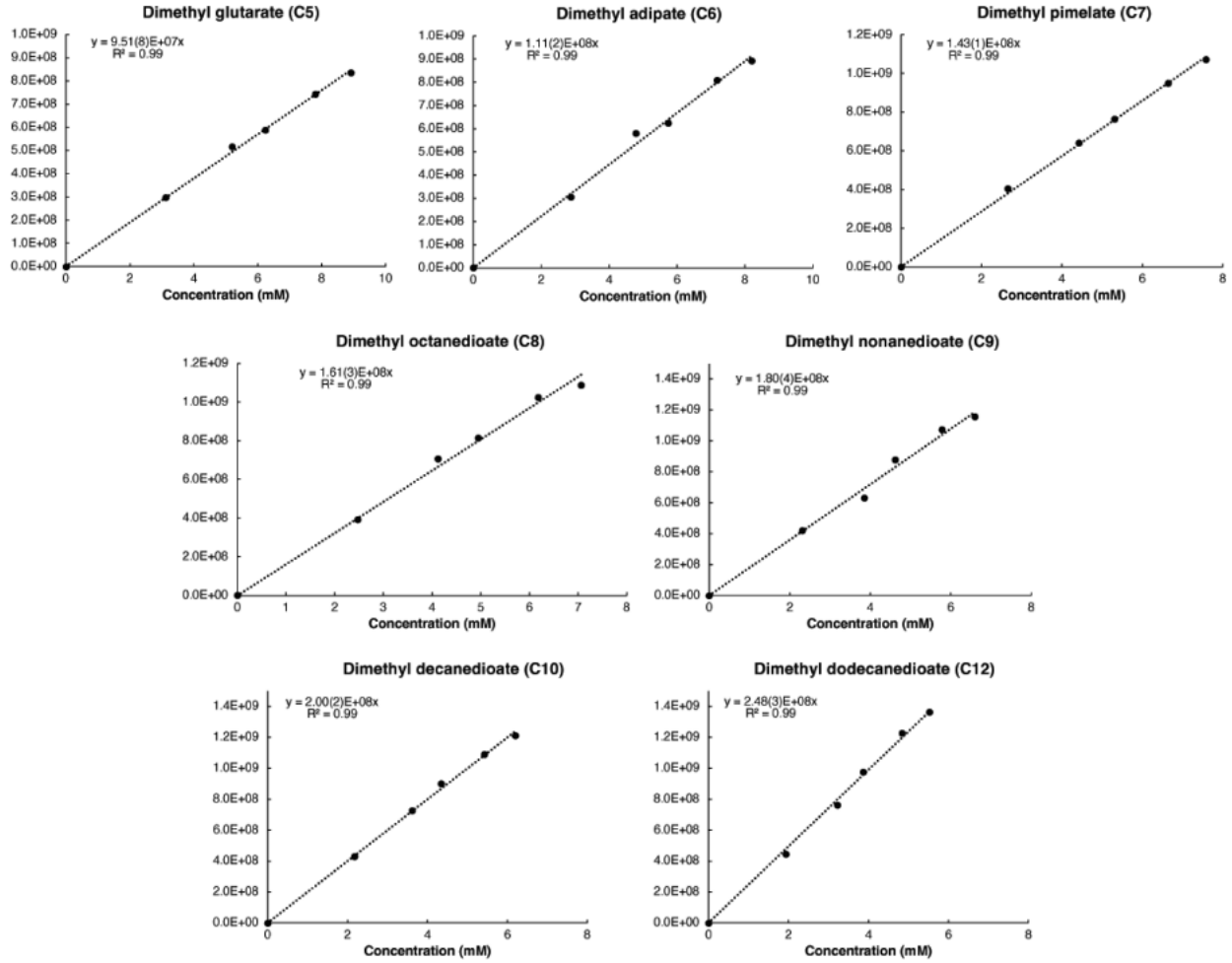

Figure S3. Calibration curves determined by the standard methanol-esterified products.

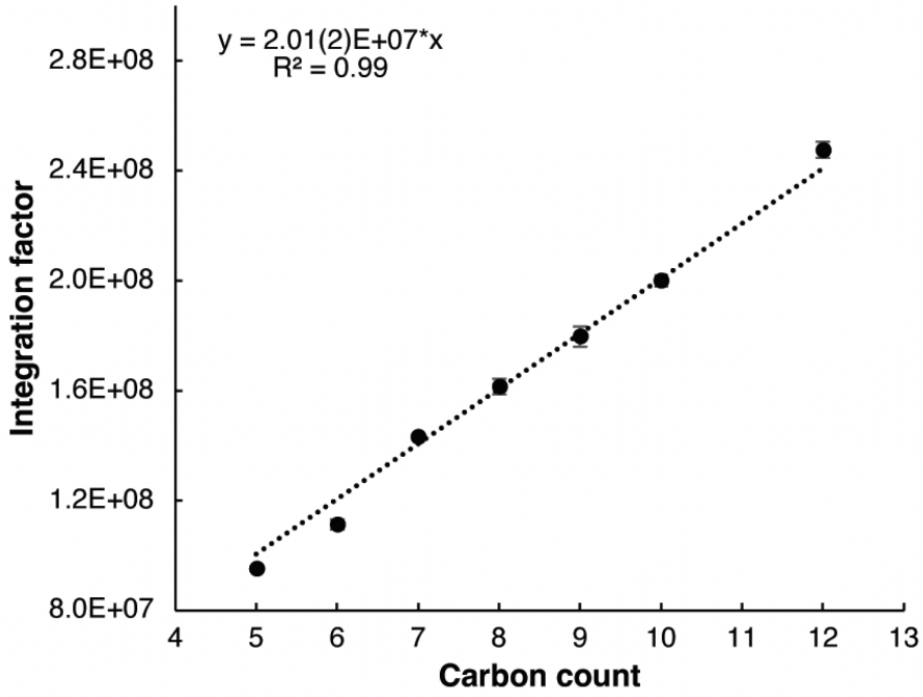

Figure S4. The correlation between carbon count of the methanol-esterified product and corresponding GC-MS integration factor.

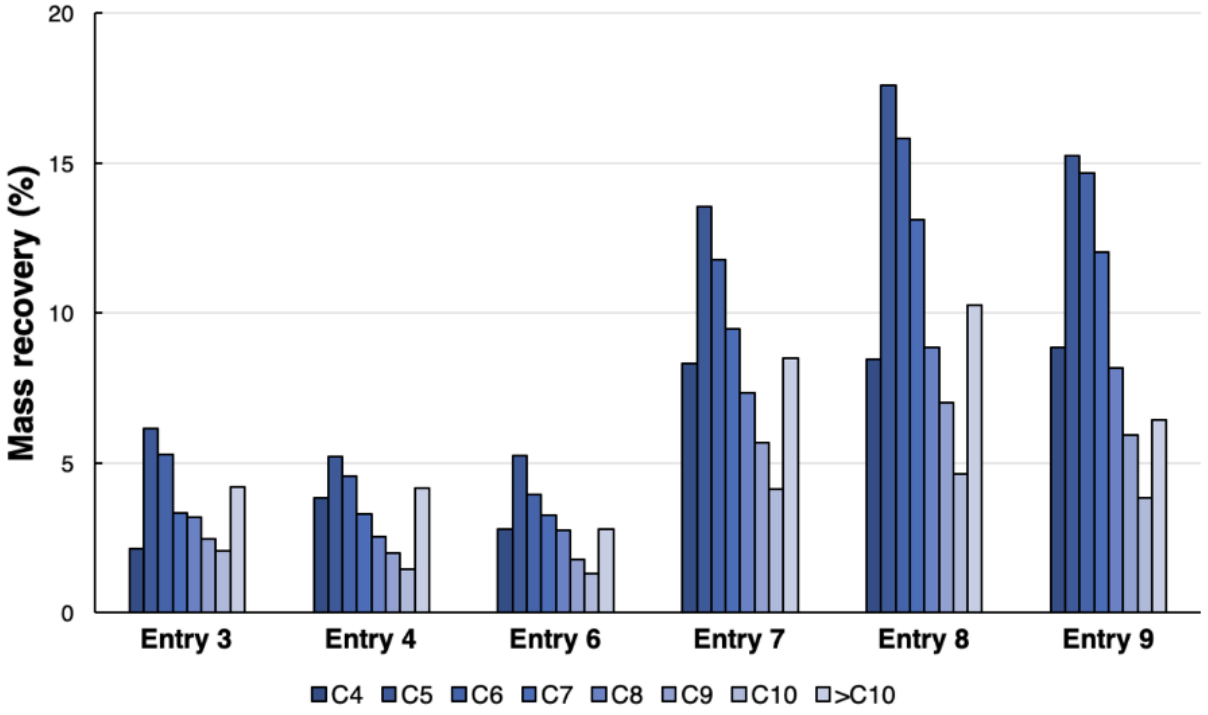

Figure S5. The distribution of diacid products after model LDPE degradation under different catalytic conditions. (Referring to entries in Table S3, see below).

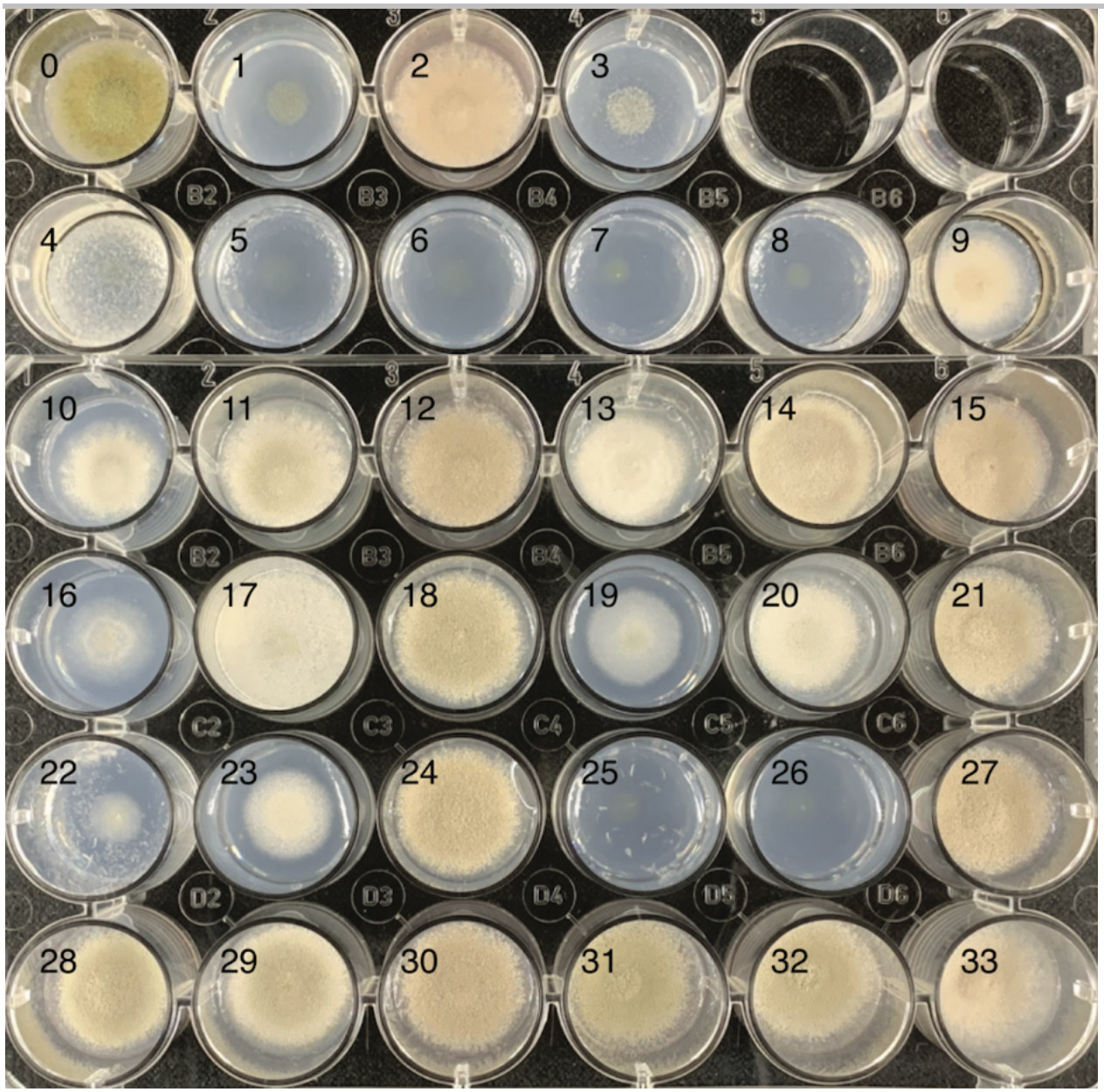

Figure S6. 24-well plates showing toxicity of dicarboxylic acids and reaction catalysts to fungi. 1.0 x 10^6 spores of A. nidulans FGSC A4 were inoculated into each well containing 2 mL (0) GMM; (1) MM; (2) GMM + 3% v/v DMSO; (3) MM + 3% v/v DMSO; (4-6) GMM + 10/5/1 g L^{-1} NHPI; (7-9) GMM + 10/5/1 g L^{-1} phthalic acid; (10-12) GMM + 10/5/1 g L^{-1} succinic acid; (13-15) GMM + 10/5/1 g L^{-1} glutaric acid; (16-18) GMM + 10/5/1 g L^{-1} adipic acid; (19-21) GMM + 10/5/1 g L^{-1} pimelic acid; (22-24) GMM + 10/5/1 g L^{-1} suberic acid; (25-27) GMM + 10/5/1 g L^{-1} azelaic acid; (28-30) GMM + 10/5/1 g L^{-1} sebacic acid; (31-33) GMM + 10/5/1 g L^{-1} dodecanedioic acid. All diacid standards were initially dissolved in 60 µL (3% v/v) DMSO. Cultures were incubated for seven days at 37 °C.

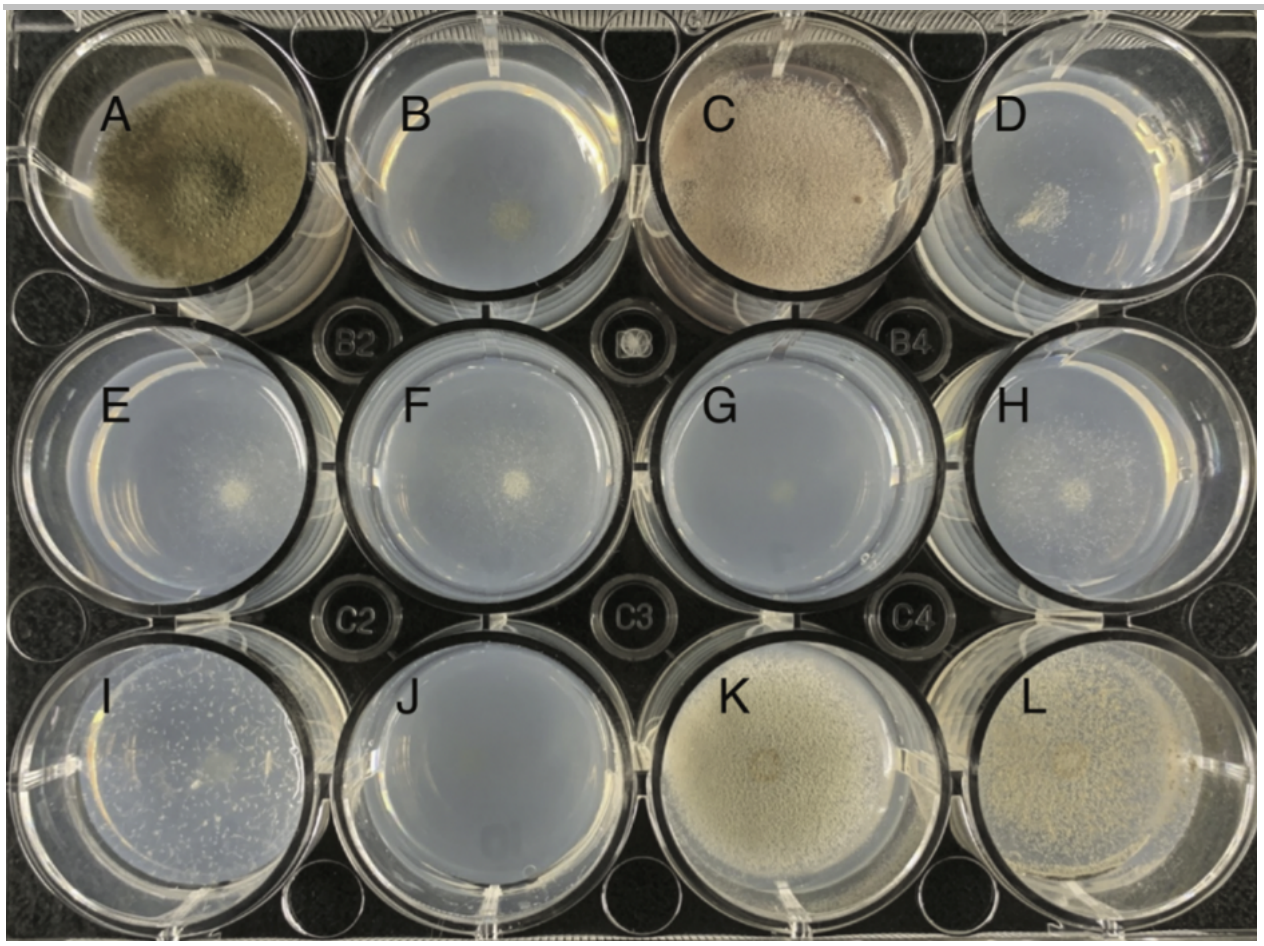

Figure S7. Fungal utilization of dicarboxylic acids as sole carbon sources. 1.0 x 10^6 spores of *A. nidulans* FGSC A4 were inoculated into each well containing 10 mL (A) GMM; (B) MM; (C) GMM + 3% v/v DMSO; (D) MM + 3% v/v DMSO; (E) MM + 10 g L^{-1} succinic acid; (F) MM + 10 g L^{-1} glutaric acid; (G) MM + 10 g L^{-1} adipic acid; (H) MM + 10 g L^{-1} pimelic acid; (I) MM + 10 g L^{-1} suberic acid; (J) MM + 10 g L^{-1} azelaic acid; (K) MM + 10 g L^{-1} sebacic acid; (L) MM + 10 g L^{-1} dodecanedioic acid. All diacid standards were initially dissolved in 300 µL (3% v/v) DMSO. Cultures were incubated for seven days at 37 °C.

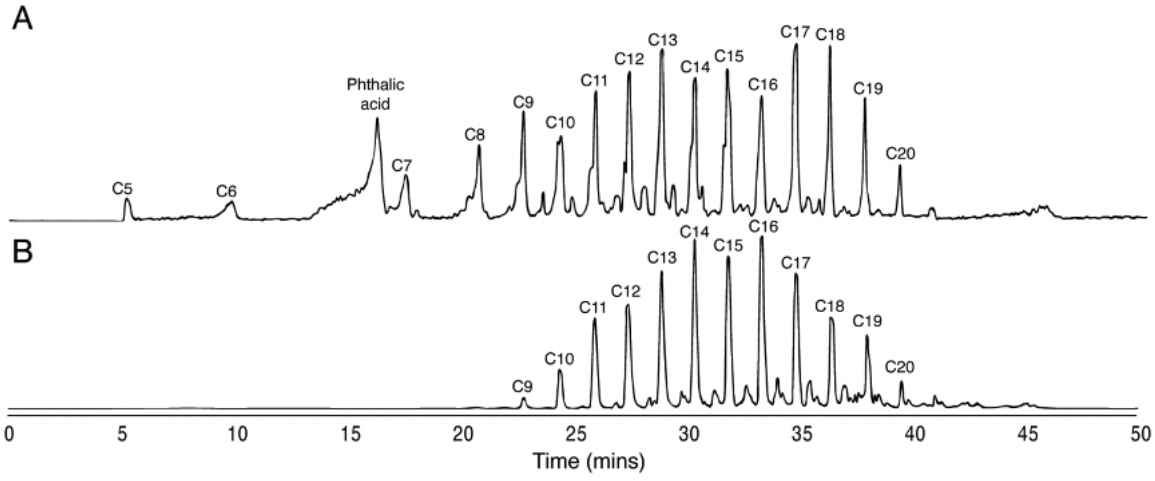

Figure S8. Paired HPLC-DAD-MS traces of (A) crude polyethylene digest and (B) polyethylene digest following pH-controlled liquid-liquid extraction. Diacid and phthalic acid peaks are annotated.

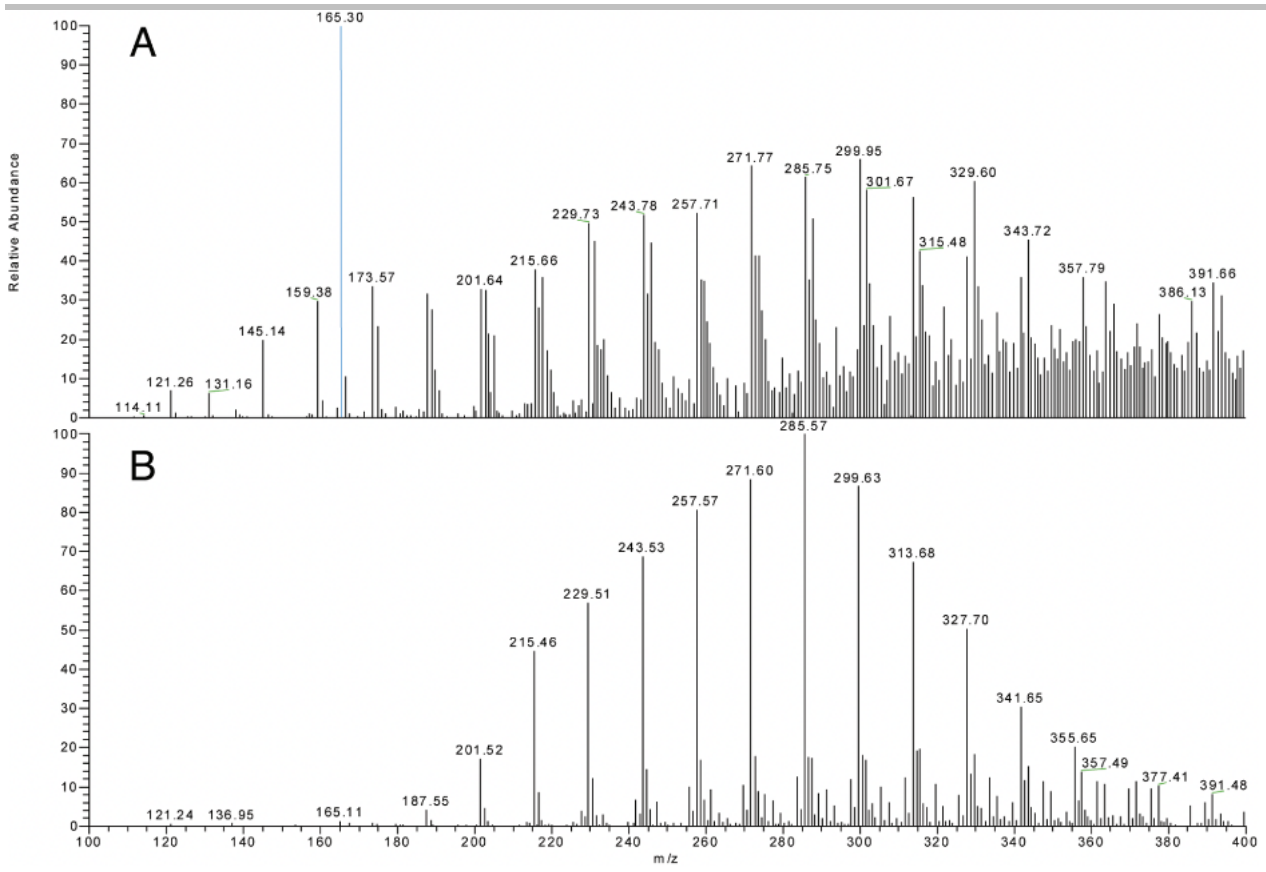

Figure S9. Mass spectra of (A) crude polyethylene digest and (B) polyethylene digest following pH-controlled liquid-liquid extraction. Differences of m/z = 14 indicate consecutive additions of methylene groups. The peak representing phthalic acid is highlighted in blue.

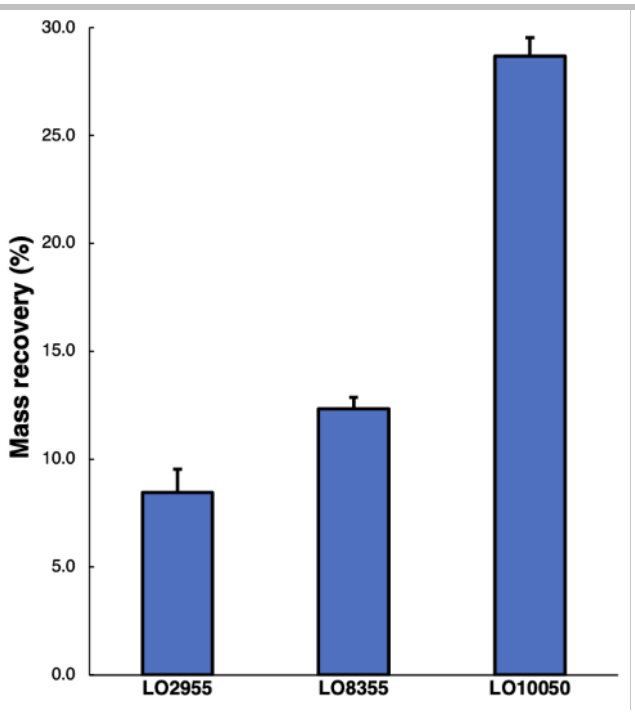

Figure S10. Comparative asperbenzaldehyde mass recoveries of strains LO2955, LO8355, and LO10050 cultured in lactose minimal media (LMM). Yields were 1.27, 1.85, and 4.30 g L^{-1} from 15 g L^{-1} of carbon source for LO2955, LO8355, and LO10050, respectively.

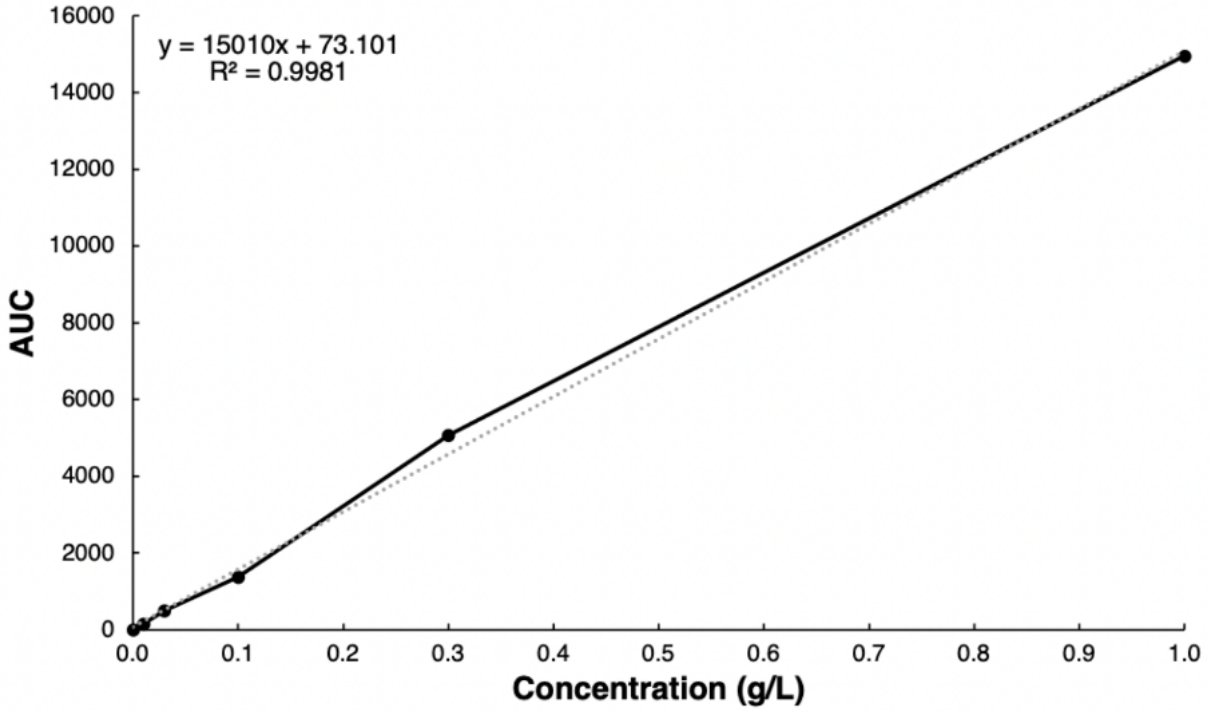

Figure S11. Standard curve of asperbenzaldehyde generated via HPLC-DAD.

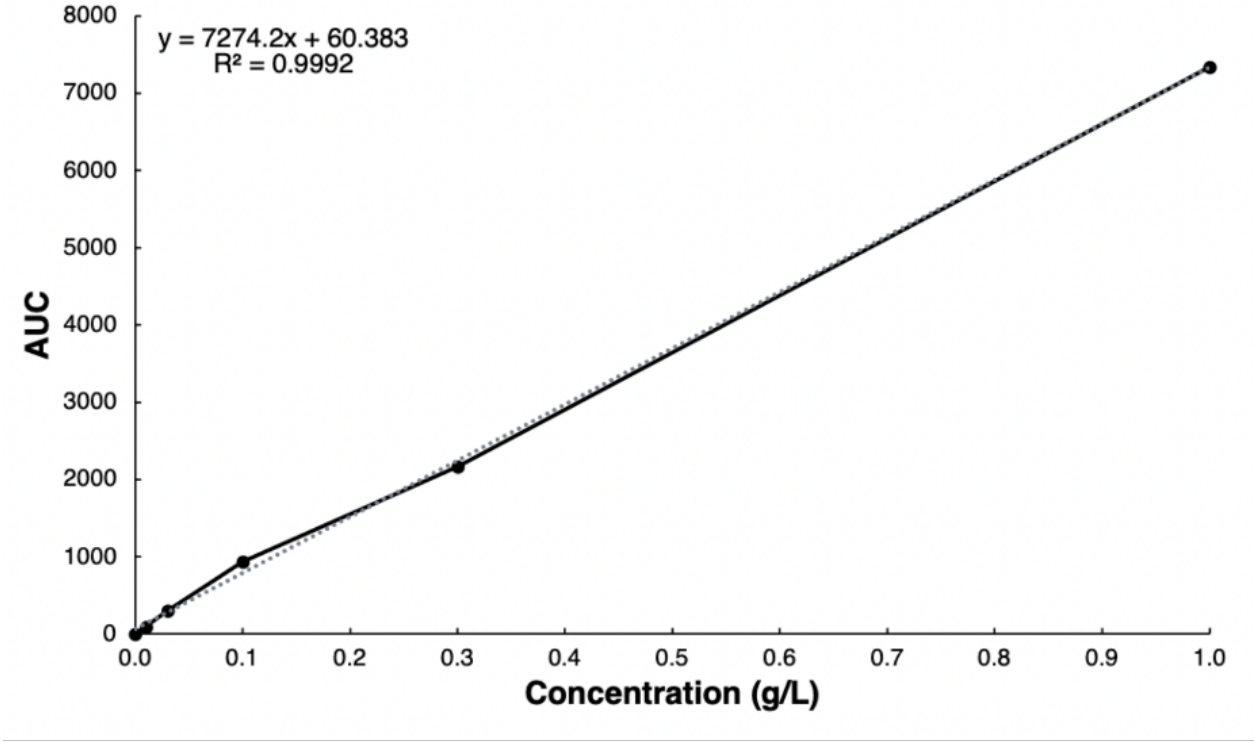

Figure S12. Standard curve of citreoviridin generated via HPLC-DAD.

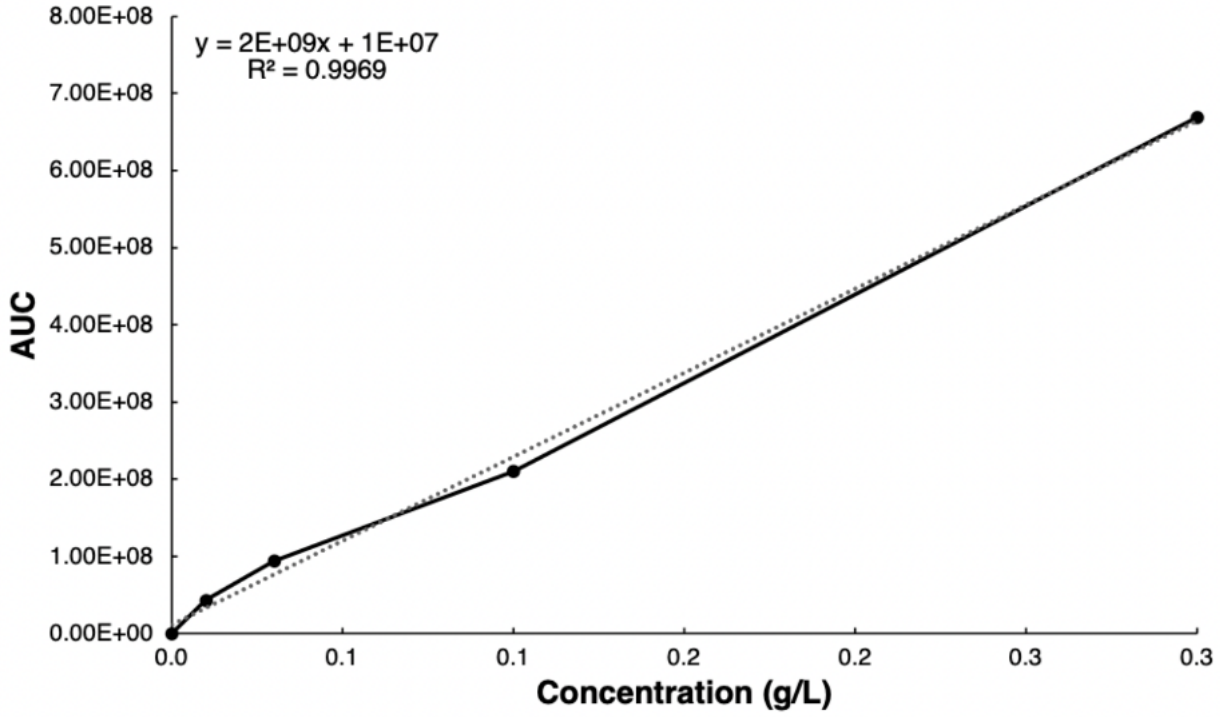

Figure S13. Standard curve of mutilin generated via HPLC-DAD-MS.

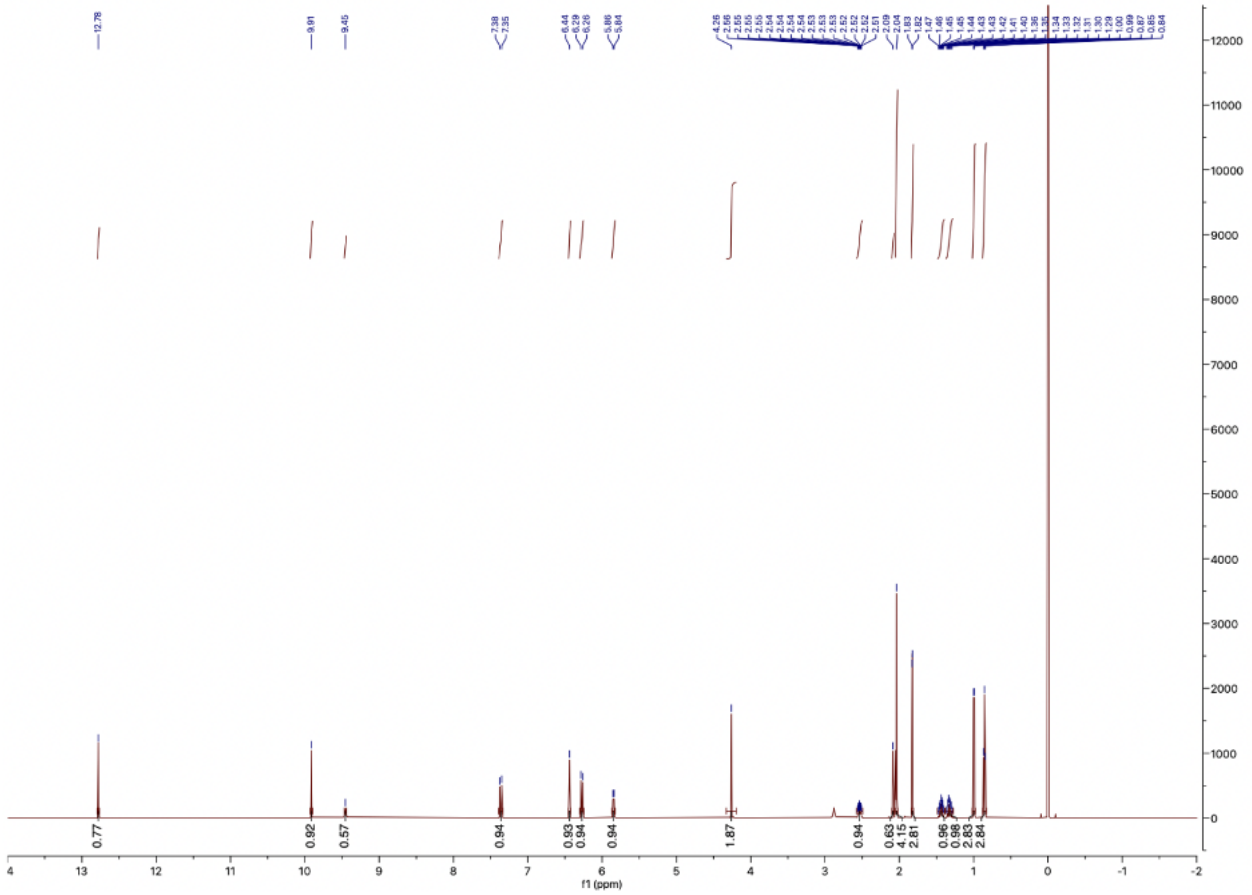

Figure S14. ^{1}H NMR spectrum of asperbenzaldehyde purified from LO10050 when cultured in liquid PMM medium. 13.3 mg of asperbenzaldehyde was dissolved in acetone-d_6.

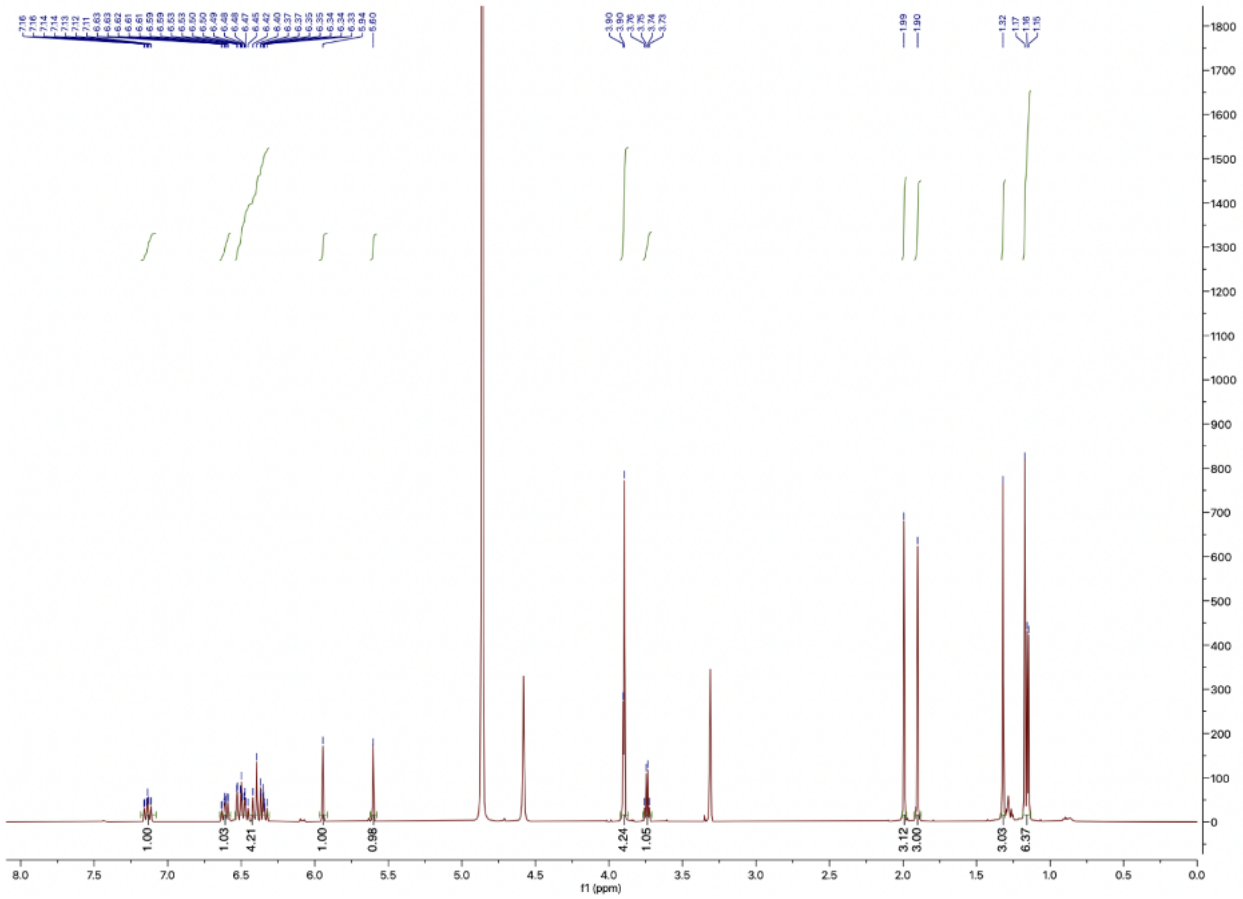

Figure S15. ^{1}H NMR spectrum of citreoviridin purified from YM192 when cultured in liquid PMM medium. 8.6 mg of citreoviridin was dissolved in methanol-d_4.

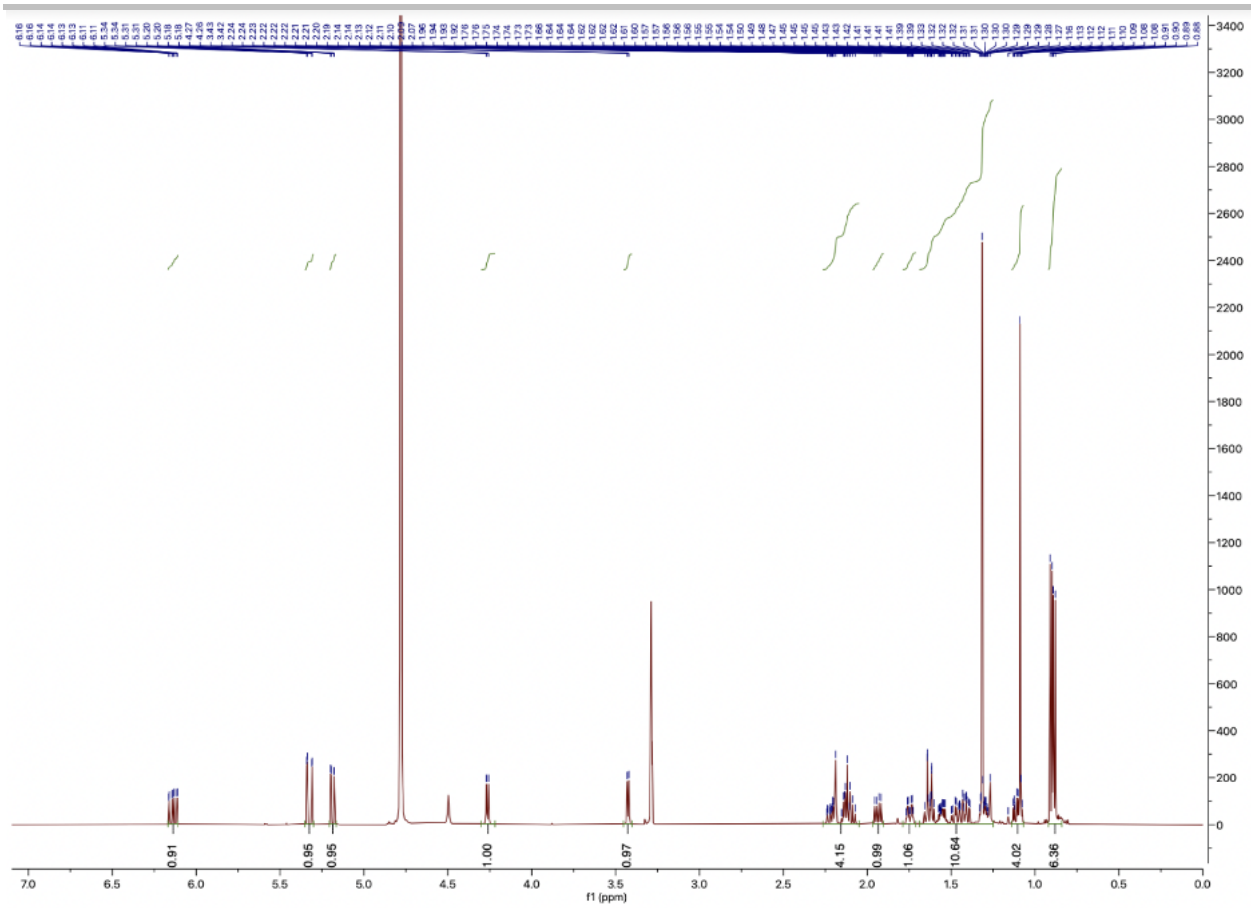

Figure S16. ^{1}H NMR spectrum of mutilin purified from YM283 when cultured in liquid PMM medium. 7.1 mg of mutilin was dissolved in methanol-d_4.

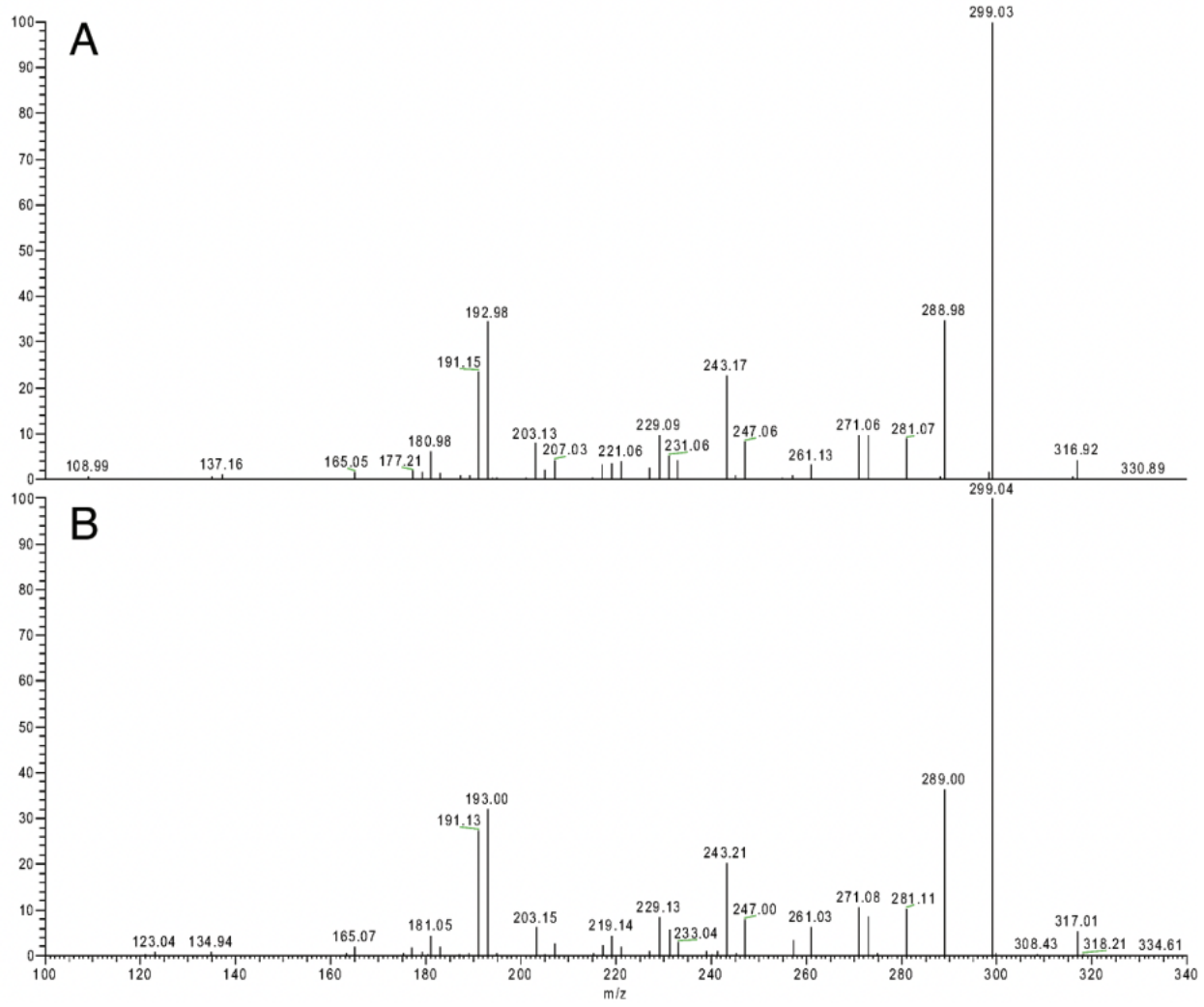

Figure S17. Tandem mass spectra of asperbenzaldehyde produced in (A) GMM and (B) PMM liquid medium.

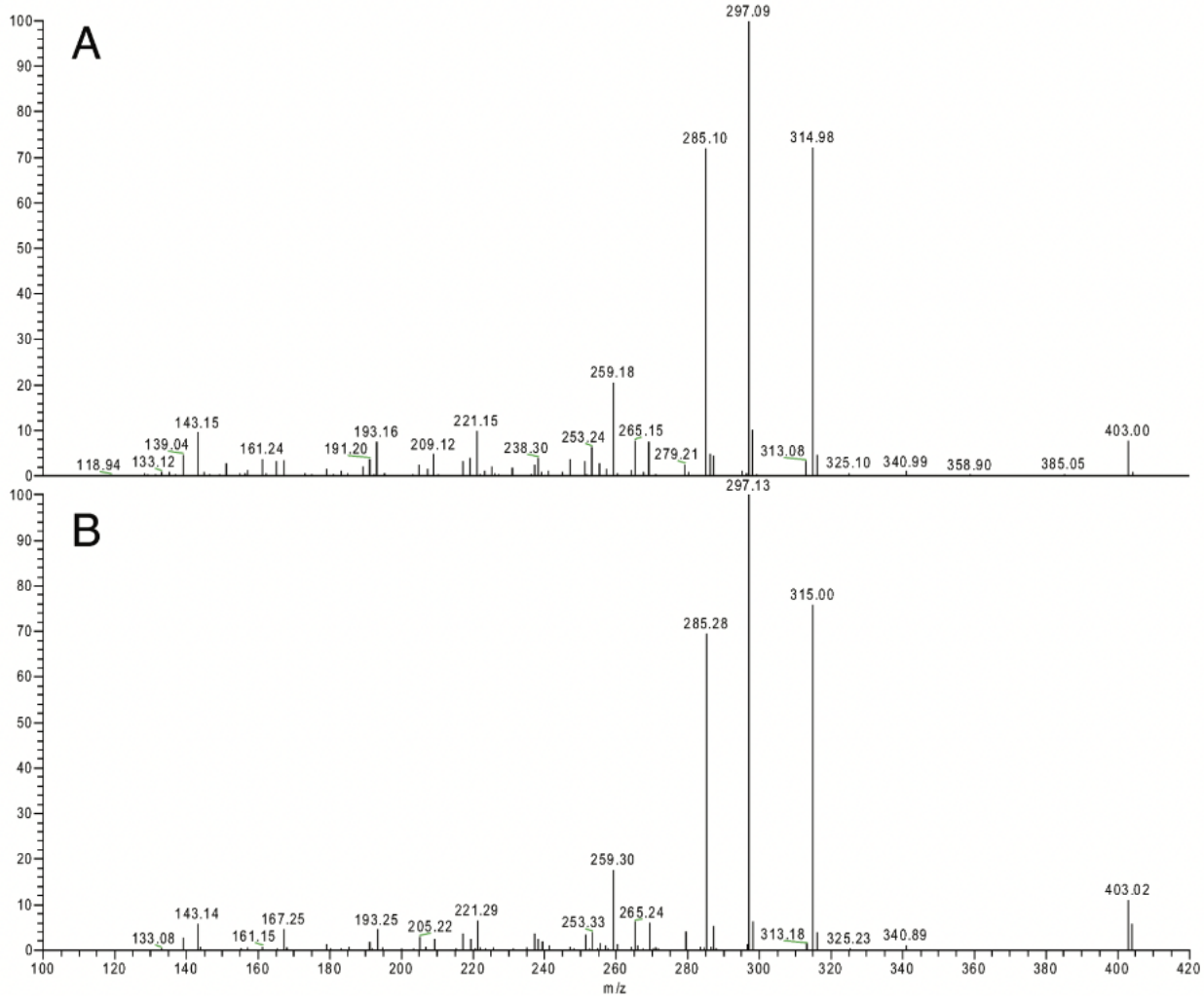

Figure S18. Tandem mass spectra of citreoviridin produced in (A) GMM and (B) PMM liquid medium.

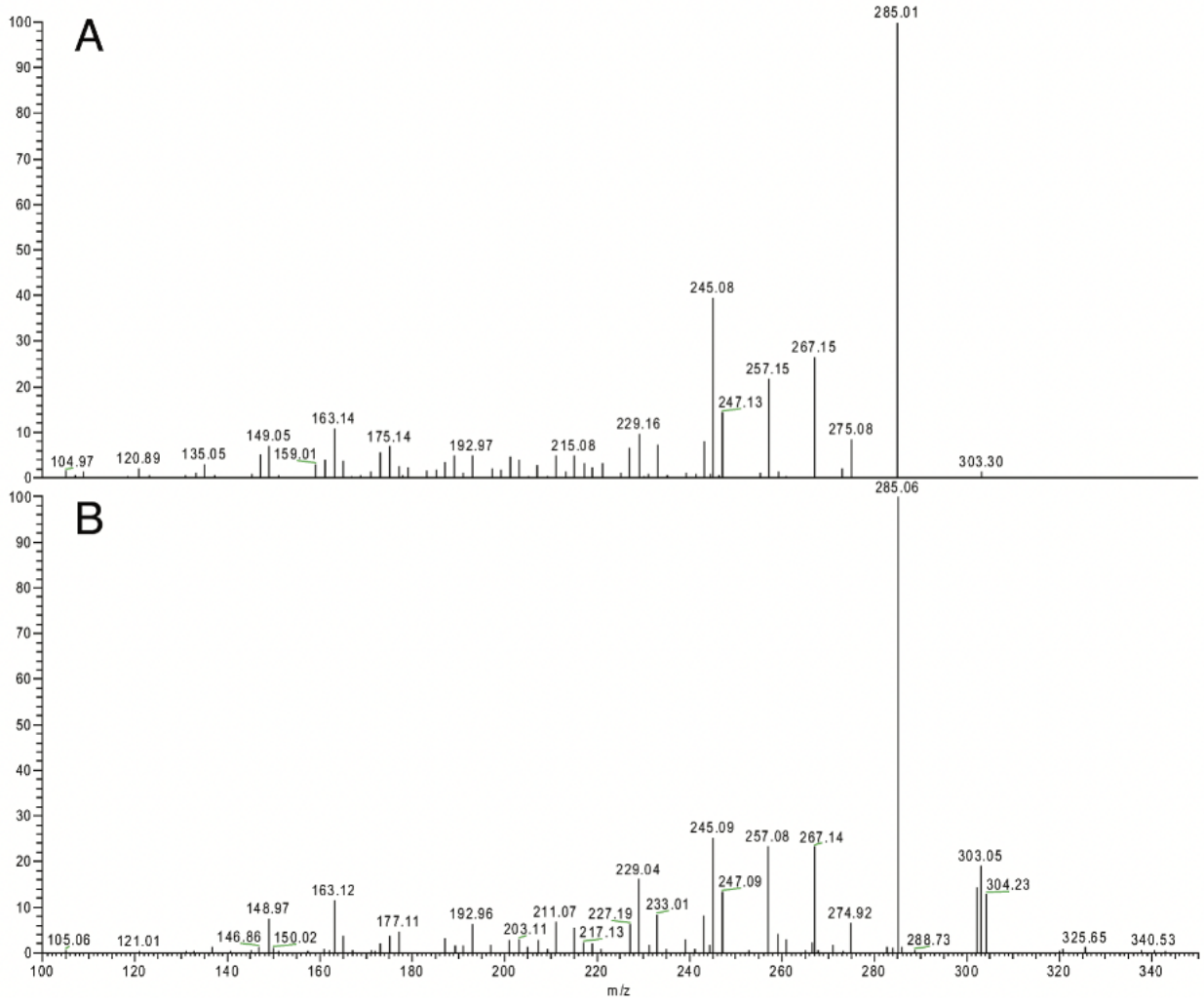

Figure S19. Tandem mass spectra of mutilin produced in (A) GMM and (B) PMM liquid medium. The m/z ≈ 303 represents the $[M+H-H_2O]^+$ ion.

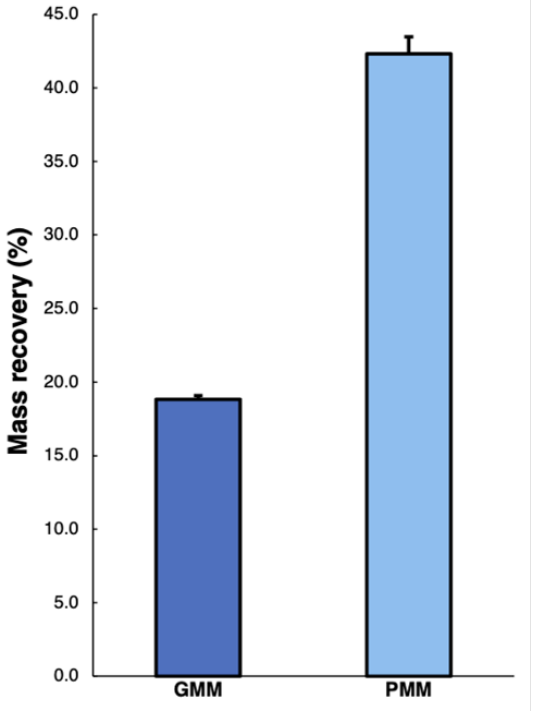

Figure S20. Asperbenzaldehyde mass recovery from strain LO10050 when cultured in liquid GMM vs. PMM (glucose- and plastics-minimal media). PMM was generated using post-consumer polyethylene digest. Yields were 1.88 and 4.23 g L^{-1} asperbenzaldehyde from 10 g L^{-1} of GMM and PMM, respectively.

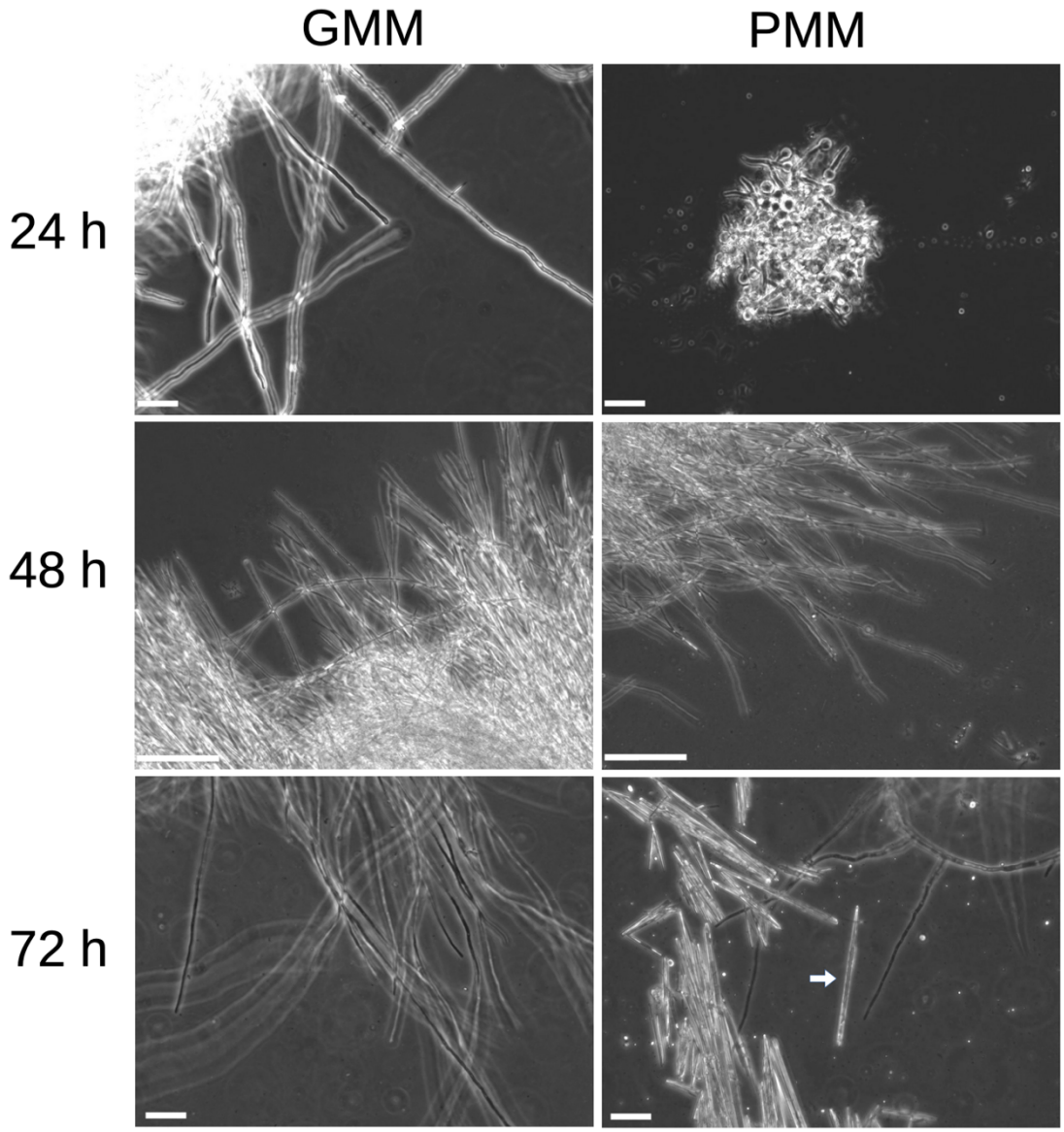

Figure S21. Phase contrast micrographs of asperbenzaldehyde-producing strain LO10050 in GMM and PMM. Cultures were grown in 10 mL liquid cultures in 30 mL Erlenmeyer flasks. Incubation time is displayed on the left. In GMM (left column), hyphal growth is extensive by 24 h. Hyphae remain healthy at 48 h but show some darkening at 72 h indicating a loss of viability. In PMM, germination of the same strain is delayed; at 24 h only short germlings are present. By 48 hours hyphal growth is robust. By 72 hours most hyphae are dark indicating that they are no longer viable. However, crystals are abundant (one of which is indicated with an arrow). These crystals match the previously reported description of asperbenzaldehyde crystals[40]. From the large amounts of asperbenzaldehyde produced under these conditions as detected via HPLC-DAD, we are confident that the crystals are asperbenzaldehyde. Asperbenzaldehyde crystals are seen occasionally in GMM, but they are much less abundant than in PMM. Scale in each panel = 25 µm.

SUPPORTING INFORMATION

Tables

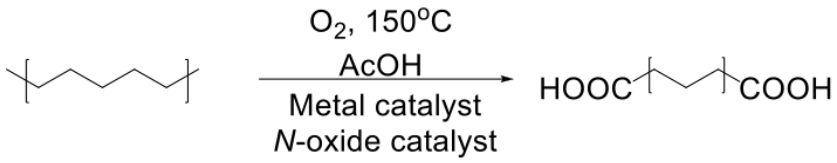

Entry[a]	O_2 Consumption (mol)	N-oxide Catalyst[b]	Metal Catalyst	Est. Average Product Size[c]
1	0.110	NH_2OH	$Co(acac)_2$	Long
2	0.093	NHS	$Co(acac)_2$	Mid-Long
3	0.093	TEMPO	$Co(acac)_2$	Long
4	0.223	NHPI	$Co(acac)_2$	Medium
5	0.148	NHPI	$Mn(acac)_2$	Long
6	0.141	NHPI	$Mn(acac)_3$	Long
7	0.167	NHPI	$Cu(acac)_2$	Long
8	0.167	NHPI	$Co(NO_2)_3$	Medium
9	0.121	NHPI	$Co(NO_2)_3$ + $Mn(NO_2)_3$	Mid-Short
10[d]	/	NHPI	$Co(acac)_2$ + $Mn(acac)_2$	/
11	0.130	TEMPO	$Co(NO_2)_3$ + $Mn(NO_2)_3$	Long

Table S1. Screening of different catalytic systems for LDPE degradation: (a) In a pressurized 300-mL Parr reactor, model LDPE (5g) was reacted with molecular oxygen (16 bars) with the presence of *N*-oxide catalyst (0.5g) and metal catalyst (0.5g of each) in acetic acid (75mL) at 150°C. The reaction was manually terminated when no more oxygen consumption happened (b) NHS = *N*-Hydroxysuccinimide; NHPI = *N*-Hydroxyphthalimide (c) Based on the relative NMR peak intensity of alpha, beta and gamma protons: short (C4-C6), mid-short (C7-C8), medium (C9-C10), mid-long (C11-C12) and long (C12+) (d) No reaction.

Carbon chain number	Integration Factor (vs mM)	R square	Standard Error
5	95082214.5	0.99	788410.3 (0.8%)
6	111304407.5	0.99	1899257.2 (1.7%)
7	143192867.3	0.99	1050684 (0.7%)
8	161441288.4	0.99	2807188.8 (1.7%)
9	179732978.1	0.99	3675148.2 (2.0%)
10	199947948.7	0.99	1879567.0 (0.9%)
12	247589859.8	0.99	2972327.8 (1.2%)
Prediction Curve: y = 20,090,725.4 x, S.E. = 235212 (1.2%)			
11	220997890.5		
13	261179431.5		
14	281207157.0		
15	301360882.5		
16	321451697.0		
17	341542333.5		
18	361633059.0		

Table S2. GCMS integration factors of corresponding methanol-esterified products: (a) Integration factors of C11, 13-18 diesters are calculated based on the correlation curve (also see Fig. S4).

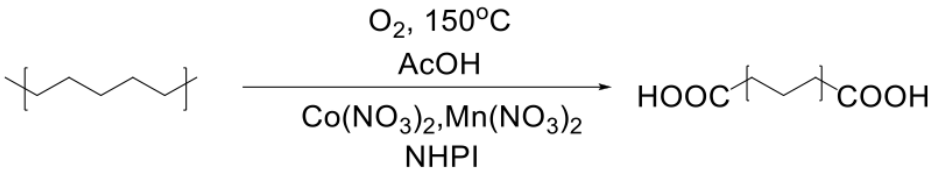

Entry[a]	O_2 Loading (bars)	O_2 Delivery cycle	O_2 Consum. (mol)	Time (hrs)	Catalysts (wt%) Co	Mn	NHPI	Mass Recy. (wt%)[b]	Molar Yield (%)[c]
1	18	1	0.127	4	10	10	10	36.0	22.4
2	6	3	0.109	6.5	10	10	10	29.0	17.8
3	2	5	0.077	7.5	10	10	10	28.8	17.5
4	2	6	0.086	9.5	10	10	10	27.0	16.2
5	2	6	0.099	8	5	5	10	26.8	16.8
6	2	6	0.095	8	2	2	10	23.8	14.3
7[d]	2	9	0.150	10.5	4	4	20	68.8	41.3
	cycle 1-6		0.095	7	2	2	10		
	cycle 7-9		0.045	3.5	2	2	10		
8[e]	2	10	0.172	11.5	6	6	20	85.7	51.6
	cycle 1-6		0.099	7	2	2	10		
	cycle 7-10		0.073	4.5	4	4	10		
9[f]	2	12	0.204	14	6	6	30	75.1	44.7
	cycle 1-6		0.095	7	2	2	10		
	cycle 7-12				4	4	20		

Table S3a. Optimization of reaction condition with reduced O_2 and catalysts loading: (a) Reaction conditions unless specified mentioned otherwise: A mixture of model LDPE (5g), catalysts, and acetic acid (75mL) was stirred in a 300-mL, oxygen-pressurized Parr reactor (with active refilling) at 150°C (b) Mass Recovery Yield (wt%) = [(Mass of diacid products)/(Mass of starting LDPE)] x 100% (c) Molar Yield (%) = [(Mass of carbon in diacid products)/(Mass of carbon in starting LDPE)] x 100% (d) Extra 2 wt% of each metal catalyst and 10 wt% of NHPI was added after 6th oxygen delivery cycle (e) Additional 4 wt% of each metal catalyst and 10 wt% of NHPI were added after 6th oxygen delivery cycle (f) Extra 4 wt% of each metal catalyst and 20 wt% of NHPI were added after 6th oxygen delivery cycle.

Entry[a]	Quantitative yield of diacids recovered from 5 grams of model LDPE (unit: g) C4	C5	C6	C7	C8	C9	C10	Heavy[b]	SUM
1	0.198	0.283	0.250	0.211	0.170	0.151	0.122	0.411	1.80
2	0.155	0.306	0.241	0.197	0.135	0.092	0.074	0.254	1.45
3	0.106	0.308	0.263	0.166	0.159	0.123	0.103	0.210	1.43
4	0.191	0.261	0.227	0.164	0.126	0.099	0.072	0.208	1.35
5	0.132	0.228	0.189	0.153	0.150	0.095	0.074	0.322	1.34
6	0.139	0.262	0.197	0.162	0.137	0.088	0.066	0.139	1.19
7	0.416	0.677	0.589	0.474	0.367	0.284	0.206	0.425	3.44
8	0.423	0.879	0.791	0.656	0.442	0.350	0.232	0.513	4.29
9	0.442	0.762	0.734	0.601	0.409	0.296	0.192	0.322	3.76

Table S3b. The yield of diacid products after model LDPE degradation under different catalytic conditions: (a) All entries are referred to entries in Table S3a (b) "Heavy" portion = a mixture of diacids comprises linear products of mass > C10.

Entry[a]	Time (hrs)	O_2 Loading (bars)	O_2 Delivery cycle	O_2 Consumption (mol)	Mass Recovery (wt%)	Molar Yield (%)
1[b]	10.5	2	10	0.172	35.9	21.8
2[c]	11.5	2	11	0.199	62.8	38.5
3[d]	11	2	10	0.168	54.6	33.6
4[e]	10.5	2	10	0.182	58.2	35.5

Table S4a. The degradation of post-consumer PE waste using our optimized condition (entry 8 in table S3): (a) Various of post-consumer PE waste was investigated using our optimized protocol (entry 8 in table S3) (b) LDPE Plastic grocery tag was used (c) HDPE Milk jug was used (d) LDPE Laboratory squeeze bottle was used (e) Plastic waste collected from Santa Catalina Island was used.

Entry[a]	Quantitative yield of diacids recovered from 5 grams of PE waste (unit: g)								
	C4	C5	C6	C7	C8	C9	C10	Heavy	SUM
1	0.183	0.313	0.311	0.237	0.210	0.171	0.123	0.244	1.79
2	0.533	0.447	0.423	0.345	0.285	0.245	0.199	0.665	3.14
3	0.461	0.374	0.369	0.290	0.256	0.222	0.178	0.582	2.73
4	0.344	0.506	0.715	0.218	0.210	0.180	0.150	0.584	2.91

Table S4b. The yield of diacid products after post-consumer PE waste degradation using our optimized condition: (a) All entries are referred to entries in Table S4a.

SUPPORTING INFORMATION

Strain	Genotype	Engineering technique	Product
LO2955	*pyrG89*; *pyroA4*, *nkuA*Δ::*argB*; *riboB2*, *stcJ*Δ::*AfriboB*; *afoA*Δ::*AfpyrG-alcA*(p)-*afoA*; *afoD*Δ::*AfpyroA*	*alcA*(p) promoter replacement	Asperbenzaldehyde
LO8355	*pyrG89*; *pyroA4*, *nkuA*Δ::*argB*; *riboB2*, *stcJ*Δ::*AfriboB*; *AfpyrG-alcA*(p)-*afoA*, *ptrA*^{Res}-*gpdA*(p)*alcR, afoD*Δ::*AfpyroA*	*alcA*(p) promoter replacement with added AlcR positive regulator	Asperbenzaldehyde
LO10050	*pyrG89*; *pyroA4*, *nkuA*Δ::*argB*; *riboB2*, *afoD*Δ::*AfriboB*, *AfpyroA-gpdA*(p)-*afoA*, *yA*Δ::*AtpyrG-afoE*(p)-*afoA*, *stcA-stcW*Δ, *easA-easD*Δ	Positive feedback loop	Asperbenzaldehyde
YM192	*pyrG89*; *pyroA4*; *nkuA*::*argB*; *riboB2*; *stcA-stcW*Δ; *afoA*::*alcA*(p)-*afoA*; *afoC-afoG*Δ::*ctvA-ctvB-ctvC-ctvD-AfpyrG*	Heterologous expression (*A. terreus* var. *aureus* origin)	Citreoviridin
YM283	*pyrG89*; *pyroA4*; *nkuA*::*argB*; *riboB2*; *stcA-stcW*Δ; *afoA*::*alcA*(p)-*afoA*; *afoB-afoG*Δ::*pl_ggs-cyc-p450_1-p450_2-sdr-AfpyroA*	Heterologous expression (*Clitopilus passeckerianus* origin)	Mutilin

Table S5. Names, genotypes, genetic engineering techniques, and SM products of strains used in this study.

Position	Chemical shift (ppm)	Chemical shift, literature (ppm)	Δ (ppm)	Position	Chemical shift (ppm)	Chemical shift, literature (ppm)	Δ (ppm)
1	0.85 (t, *J* = 7.5 Hz, 3H)	0.85 (t, *J* = 7.2 Hz, 3H)	0.00	**8**	6.44 (s, 1H)	6.47 (s, 1H)	0.03
2	1.29 - 1.47 (m, 2H)	1.32 - 1.43 (m, 2H)	0.03 - 0.04	**9**	9.91 (s, 1H)	9.90 (s, 1H)	0.01
3	2.54 (m, 1H)	2.53 (m, 1H)	0.01	**10**	0.99 (d, *J* = 6.7 Hz, 3H)	0.99 (d, *J* = 6.8 Hz, 3H)	0.00
4	5.85 (br d, *J* = 9.9 Hz, 1H)	5.84 (br d, *J* = 9.6 Hz, 1H)	0.01	**11**	1.82 (s, 3H)	1.82 (br s, 3H)	0.00
5	7.37 (d, *J* = 15.9 Hz, 1H)	7.36 (d, *J* = 15.6 Hz, 1H)	0.01	**12**	2.04 (s, 3H)	2.03 (s, 3H)	0.01
6	6.28 (d, *J* = 15.9 Hz, 1H)	6.27 (d, *J* = 15.6 Hz, 1H)	0.01	**13**	9.45 (br s, 1H)	9.68 (br s, 1H)	0.23
7	4.26 (s, 2H)	4.25 (s, 2H)	0.01	**14**	12.78 (s, 1H)	12.78 (s, 1H)	0.00

Table S6. Chemical shifts of ^{1}H NMR spectrum obtained for asperbenzaldehyde compared to literature values.

Position	Chemical shift (ppm)	Chemical shift, literature (ppm)	Δ (ppm)	Position	Chemical shift (ppm)	Chemical shift, literature (ppm)	Δ (ppm)
1	1.15 (d, *J* = 6.4 Hz, 3H)	1.14 (d, *J* = 6.3 Hz, 3H)	0.01	**9**	7.14 (ddd, *J* = 14.2, 11.3, 2.5 Hz, 1H)	7.13 (dd, *J* = 14.9, 11.1 Hz, 1H)	0.01
2	3.74 (q, *J* = 6.4 Hz, 1H)	3.73 (q, *J* = 6.3 Hz, 1H)	0.01	**10**	6.30 - 6.65 (m, 5H)	6.51 (d, *J* = 14.9 Hz, 1H	-
3	3.90 (s, 1H)	3.89 (s, 1H)	0.01	**11**	5.60 (s, 1H)	5.60 (s, 1H)	0.00
4	5.94 (s, 1H)	5.94 (br s, 1H)	0.00	**12**	1.17 (s, 3H)	1.16 (s, 3H)	0.01
5	6.30 - 6.65 (m, 5H)	6.40 (d, *J* = 15.2 Hz, 1H)	-	**13**	1.32 (s, 3H)	1.31 (s, 3H)	0.01
6	6.30 - 6.65 (m, 5H)	6.33 (dd, *J* = 15.2, 9.7 Hz, 1H)	-	**14**	1.89 (s, 3H)	1.89 (d, *J* = 1.2 Hz, 3H)	0.00
7	6.30 - 6.65 (m, 5H)	6.61 (dd, *J* = 14.7, 9.7 Hz, 1H)	-	**15**	1.99 (s, 3H)	1.99 (s, 3H)	0.00
8	6.30 - 6.65 (m, 5H)	6.47 (dd, *J* = 14.7, 11.1 Hz, 1H)	-	**16**	3.90 (s, 3H)	3.89 (s, 3H)	0.01

Table S7. Chemical shifts of ^{1}H NMR spectrum obtained for citreoviridin compared to literature values.

Position	Chemical shift (ppm)	Chemical shift, literature (ppm)	Δ (ppm)	Position	Chemical shift (ppm)	Chemical shift, literature (ppm)	Δ (ppm)
1	1.07 - 1.14 (m, 1H), 1.25 - 1.68 (m, 5H)	1.07 - 1.16 (m, 1H), 1.27 - 1.70 (m, 5H)	0.00 - 0.02, 0.02 - 0.02	**9**	1.94 (dd, *J* = 15.8, 7.7 Hz, 1H), 1.63 (d, *J* = 15.7 Hz, 1H)	1.95 (dd, *J* = 15.8, 7.6 Hz, 1H), 1.64 (d, *J* = 15.8 Hz, 1H)	0.01, 0.01
2	2.06 - 2.26 (m, 2H)	2.06 - 2.27 (m, 2H)	0.00 - 0.01	**10**	4.26 (d, *J* = 7.7 Hz, 1H)	4.27 (d, *J* = 7.6 Hz, 1H)	0.01
3	2.19 (s, 1H)	2.20 (s, 1H)	0.01	**11**	1.32 (s, 3H)	1.33 (s, 3H)	0.01
4	1.72 - 1.77 (m, 1H)	1.72 - 1.78 (m, 1H)	0.00 - 0.01	**12**	0.89 (d, *J* = 7.2 Hz, 3H)	0.90 (d, *J* = 7.3 Hz, 3H)	0.01
5	1.06 - 1.16 (m, 1H), 1.25 - 1.68 (m, 5H)	1.07 - 1.16 (m, 1H), 1.27 - 1.70 (m, 5H)	0.01, 0.02 - 0.02	**13**	0.90 (d, *J* = 7.0 Hz, 3H)	0.91 (d, *J* = 7.0 Hz, 3H)	0.01
6	1.06 - 1.16 (m, 1H), 1.25 - 1.68 (m, 5H)	1.07 - 1.16 (m, 1H), 1.27 - 1.70 (m, 5H)	0.01, 0.02 - 0.02	**14**	1.09 (s, 3H)	1.10 (s, 3H)	0.01
7	2.16 (m, 1H)	2.14 (m, 1H)	0.02	**15**	6.14 (dd, *J* = 18.0, 11.3, 1H)	6.15 (dd, *J* = 17.8, 11.2 Hz, 1H)	0.01
8	3.43 (d, *J* = 6.1 Hz, 1H)	3.44 (d, *J* = 6.1 Hz, 1H)	0.01	**16**	5.32 (dd, *J* = 18.0 1.5 Hz, 1H), 5.19 (dd, *J* = 11.2, 1.5 Hz, 1H)	5.34 (dd, *J* = 17.8, 1.4 Hz, 1H), 5.20 (dd, *J* = 11.2, 1.4 Hz, 1H)	0.02, 0.01

Table S8. Chemical shifts of ^{1}H NMR spectrum obtained for mutilin compared to literature values.

References

[1] P. M. Osterberg, J. K. Niemeier, C. J. Welch, J. M. Hawkins, J. R. Martinelli, T. E. Johnson, T. W. Root, S. S. Stahl, *Org. Proc. Res. Dev*. **2015**, *19*, 1537-1543.
[2] S. H. Hutner, L. Provasoli, A. Schatz, C. P. Haskins, *Proc. Am. Phil. Soc.* **1950**, *94*, 152–170.

Author Contributions

T.J.W. (equal) and C.C.C.W. (equal) conceived the idea and supervised the project. Y.C. (lead) performed the catalytic degradation experiments. B.R.O. (equal), C.E.O. (equal), and Y.M.C. (equal) conducted fungal strain engineering. C.R. (lead) implemented metabolic profiling, compound purification, and characterization. B.R.O. (equal) and C.E.O. (equal) imaged fungal strains. C.R. (equal), Y.C. (equal), C.E.O. (supporting), B.R.O. (supporting), T.J.W. (equal), and C.C.C.W. (supporting) contributed to writing and revising the manuscript.